

# KEY PROPERTIES IN PLASMA RESEARCH MODELLING AND MEASUREMENTS

Igor D. Kaganovich<sup>(a)</sup> and Yevgeny Raitses<sup>(a)</sup>

C. Swanson<sup>(a)</sup>, V.I. Demidov<sup>(c)</sup>, A. Mustafaev<sup>(d)</sup>,  
A.V. Khrabrov<sup>(a)</sup>, M. Campanell<sup>(a)</sup>, H. Wang<sup>(a)</sup>,  
D. Sydorenko<sup>(b)</sup>,

<sup>(a)</sup>Princeton Plasma Physics Laboratory, Princeton, NJ

<sup>(b)</sup> *Department of Physics, University of Alberta, Canada*

<sup>(c)</sup> *University of West Virginia, USA*

<sup>(d)</sup> *St. Petersburg Mining University, Russia*



# Outline

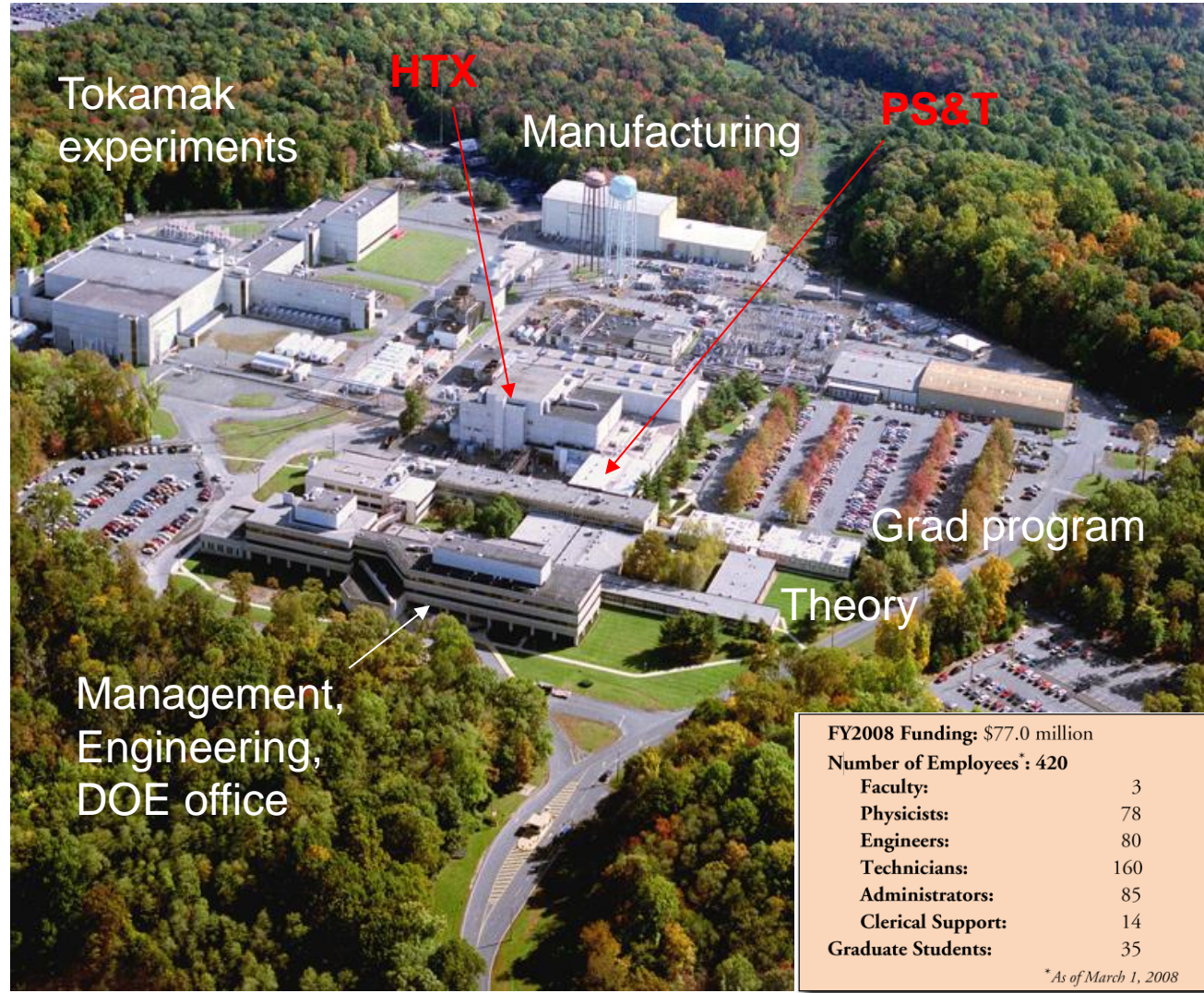
---

- Introduction
  - PPPL
  - Heavy Ion Fusion Program
  - Plasma applications where SEE is important
- SEY properties: modelling
  - PIC codes; Examples of simulations
- SEY properties: experiments
  - Experimental setups; Example of measurements of SEY

# Prof. Lyman Spitzer founded PPPL in 1951 for the Matterhorn Project on magnetic fusion



## Spitzer's Stellarator



FY2008 Funding: \$77.0 million

Number of Employees\*: 420

Faculty:	3
Physicists:	78
Engineers:	80
Technicians:	160
Administrators:	85
Clerical Support:	14
Graduate Students:	35

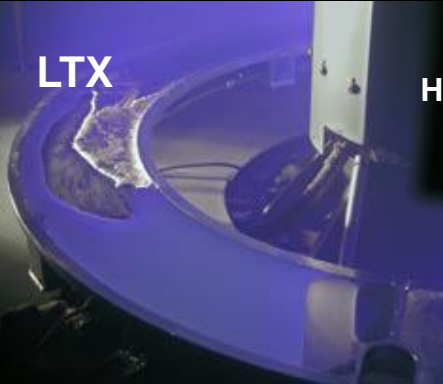
\*As of March 1, 2008



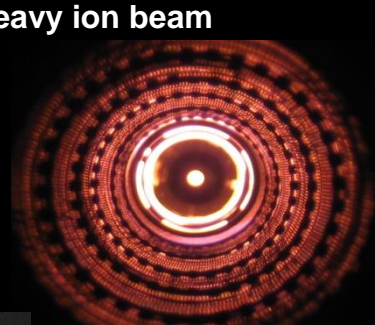
# Princeton Plasma Physics Laboratory



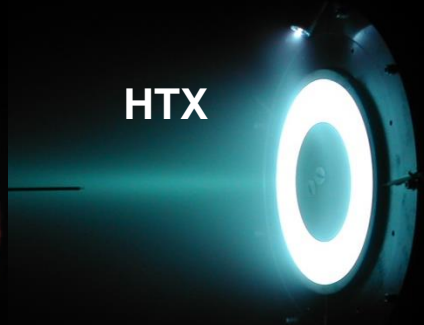
**Tokamak (NSTX)**



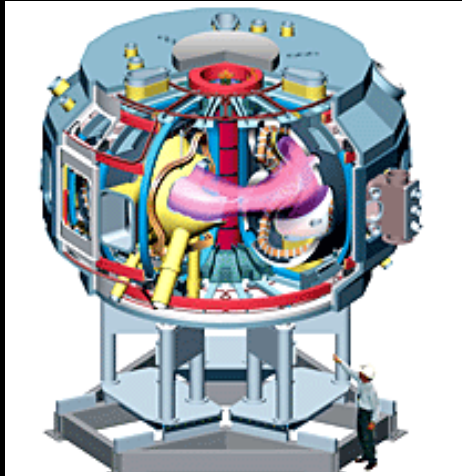
**LTX**



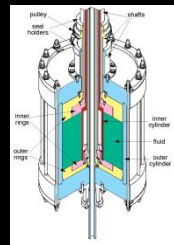
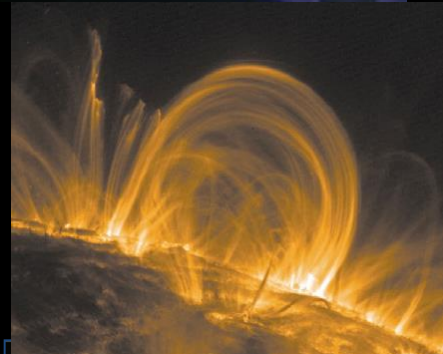
**Heavy ion beam**



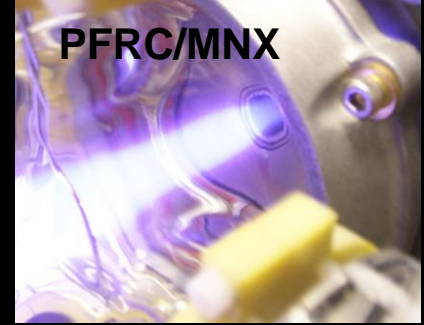
**HTX**



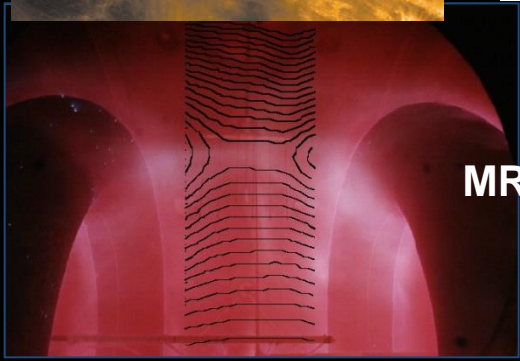
**Stellarator (NCSX)  
in 2010**



**MRI**



**PFRC/MNX**



**MRX**



# Heavy Ion Fusion Program

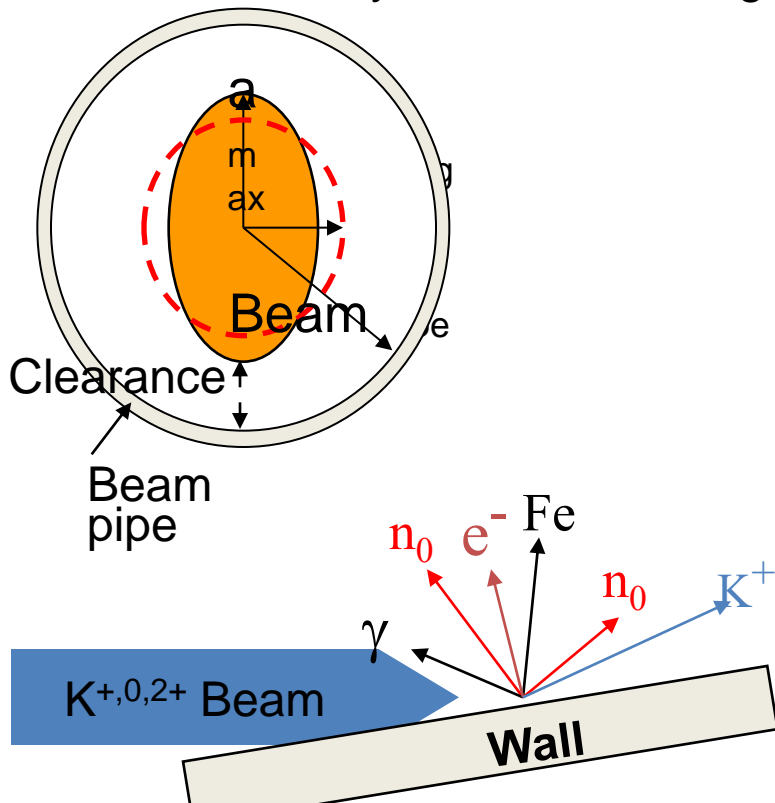
- Collaboration between LBNL, LLNL, PPPL
- Goal to produce high intensity ion beam as driver for inertial fusion.

## High Current Experiment (HCX)

Beam with  $\sim 100V$  self potential

SEY studies for ion beams A. Molvik

Gas Ionization by Ion Beam: I. Kaganovich



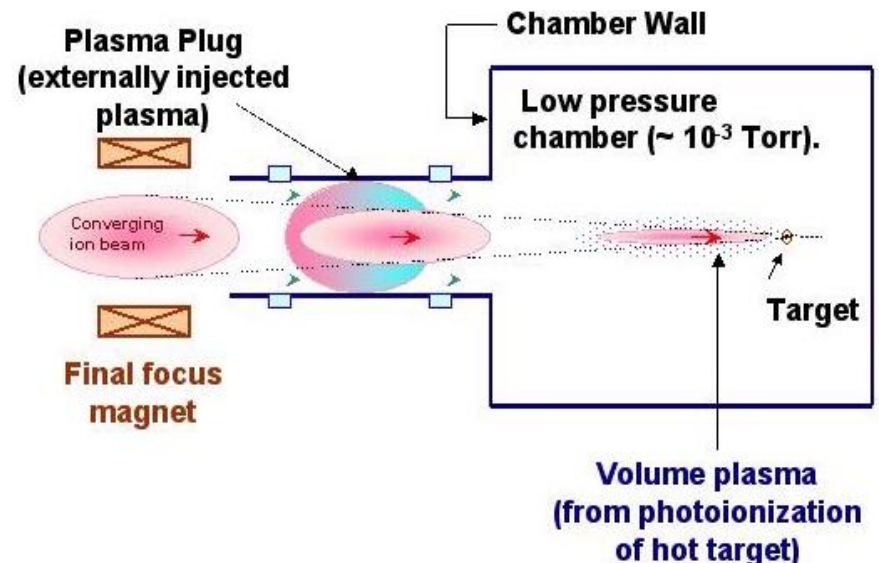
## Neutralized Drift Compression Experiment (NDCX)

Beam Compression in plasma

$\sim 70$  longitudinal,  $\sim 100s$  times radial

Experiments: P. Roy, P. Seidl

Plasma neutralization theory: I. Kaganovich



# Plasma-wall interaction in the presence of strong electron-induced secondary electron emission (SEE)

---

- Any plasma with electron temperatures above 20 eV for dielectric walls, and above 50-100 eV for metal walls is subject to strong secondary electron emission (SEE) effects:

Hall thrusters and Helicon thrusters

Hollow cathodes for high power microwave electronics

Multipactor breakdown and surface discharges

Space plasmas and dusty plasmas

Fusion plasmas

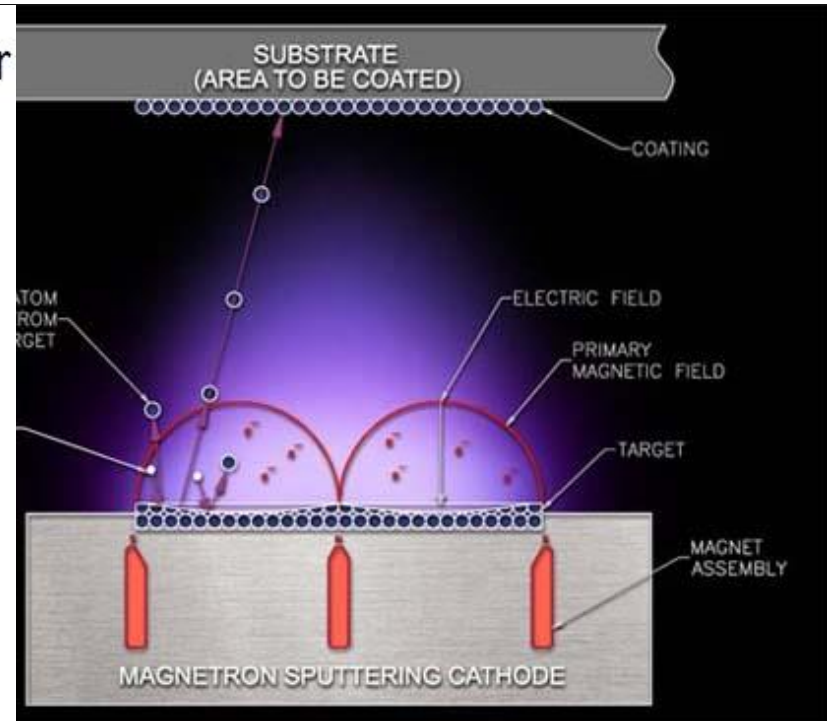
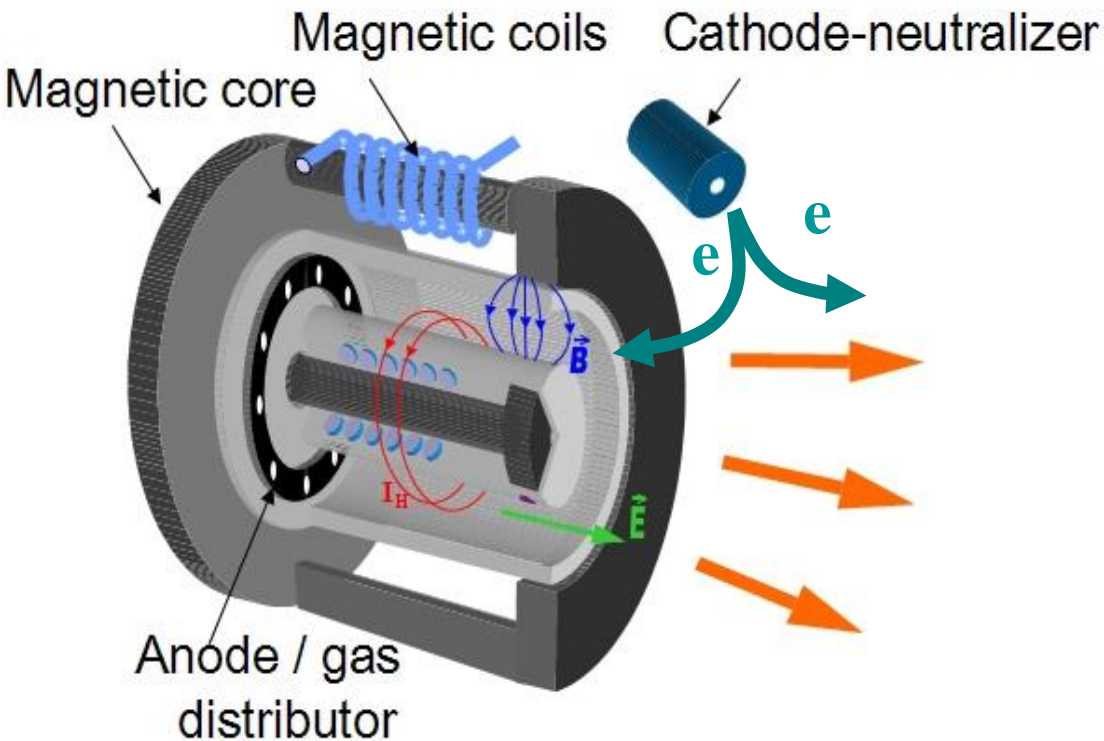
Plasma processing discharges with RF or DC bias

- Strong secondary electron emission from the floating walls can alter plasma-wall interaction and change plasma properties.
- Strong SEE can significantly increase electron heat flux from plasma to the wall leading to: 1) wall heating and evaporation and 2) plasma cooling.

# Plasma applications where SEE is important

Hall Thruster discharge: used for electric propulsion

Magnetron discharge: used for deposition, plasma switch for electric grid



From: [www.angstromsciences.com](http://www.angstromsciences.com)

# Modelling of SEE in plasma research

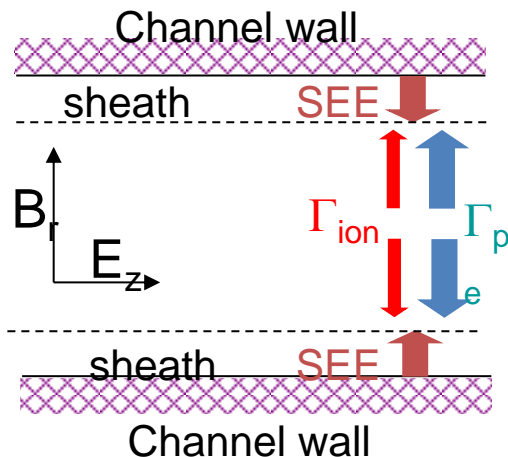
- **3D BEST PIC code:** includes electromagnetic (Darwin scheme) and electrostatic modules.

<https://nonneutral.pppl.gov/>

- **3D LSP code** includes electromagnetic and electrostatic modules. In collaboration with Voss Scientific.

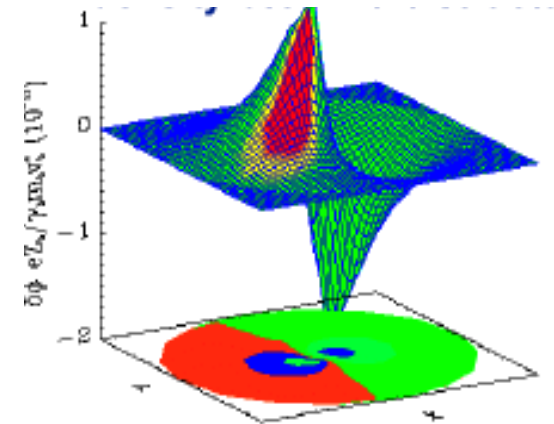
- **1-2D PIC code EDIPIC.** Implemented electron-atom scattering, ionization, and excitation as well as electron-ion and electron-electron collisions, complex SEY models.

<https://w3.pppl.gov/~ikaganov>

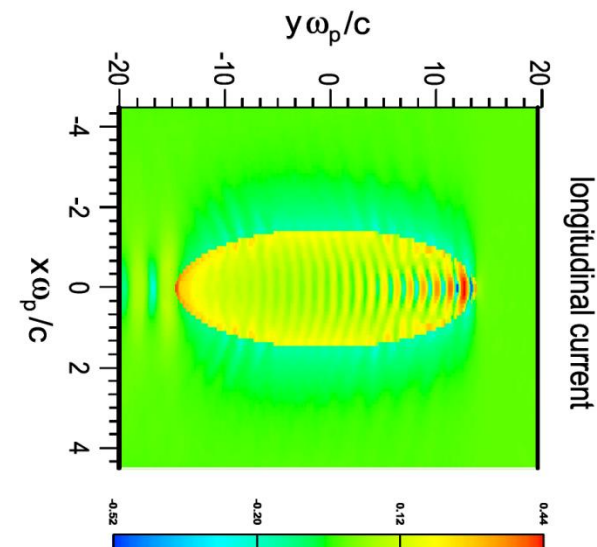


SEE electron effects on sheath and electron energy distribution functions  
5 recent PRLs

two-stream instability



electrons during neutralization

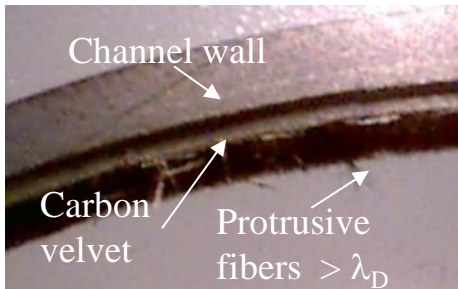


# Plasma properties can be changed by applying engineered materials to the surface

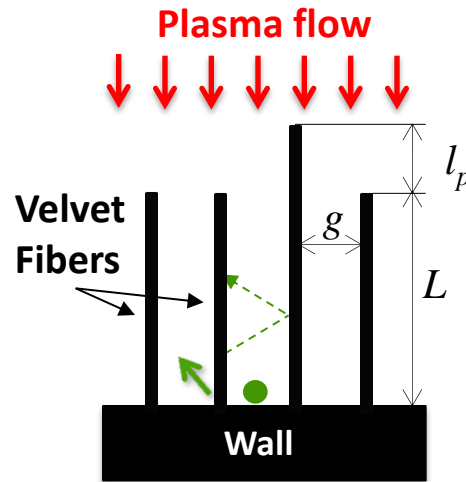


Application of carbon velvet to channel walls improves considerably thruster performance by reducing the electron cross-field current and by increasing nearly twice the maximum electric field in the channel compared with the conventional BN ceramic walls.

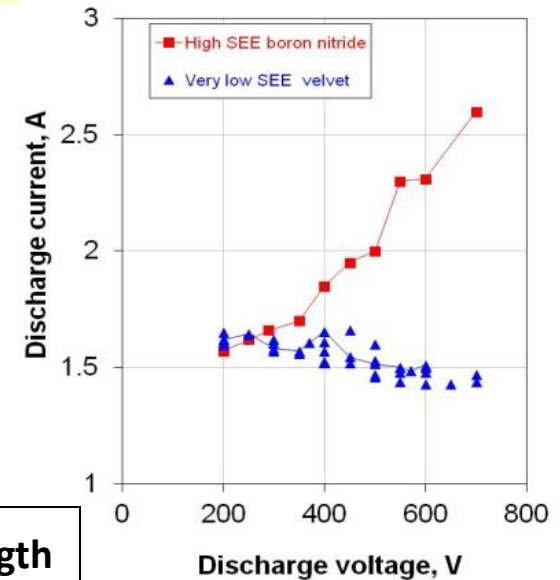
Velvet before plasma



Plasma burned out all protrusive fibers



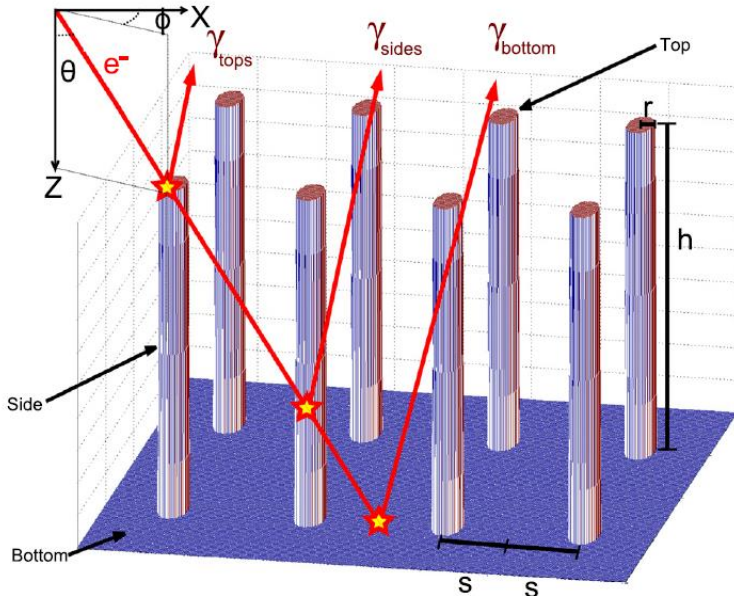
To avoid field emission  $g, l_p < \text{Debye length}$



- Velvet suppresses SEE and reduces current at high voltages (good)
  - Sharp tips can enhance field emission leading to arcing (bad)
  - Need to engineer velvet morphology so that inter fiber gaps and protrusions are located well inside the sheath to avoid damage by arcing
- Need to take into account spatial and temporal variations of sheath width due to plasma non-uniformity or instabilities

# Simulations and Theory of SEY of complex surfaces: Velvet

**Velvet: regular or irregular lattice of normally-oriented fibers**



$$u = \frac{\pi}{2} DA = 2rnh$$

$u$  dimensionless parameter,  $D$  area packing fraction,  $A$  aspect ratio of fibers,  $r$  radius of fibers,  $n$  area density of fibers,  $h$  height of fiber layer

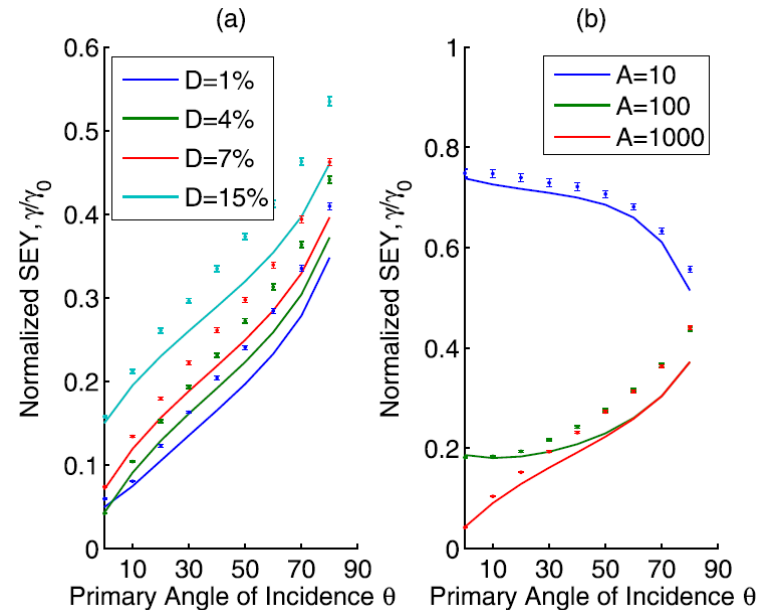
**SEY as a function of incident angle for different packing density of velvet.**

Lines: Analytic model.

Points: Monte-Carlo simulations.

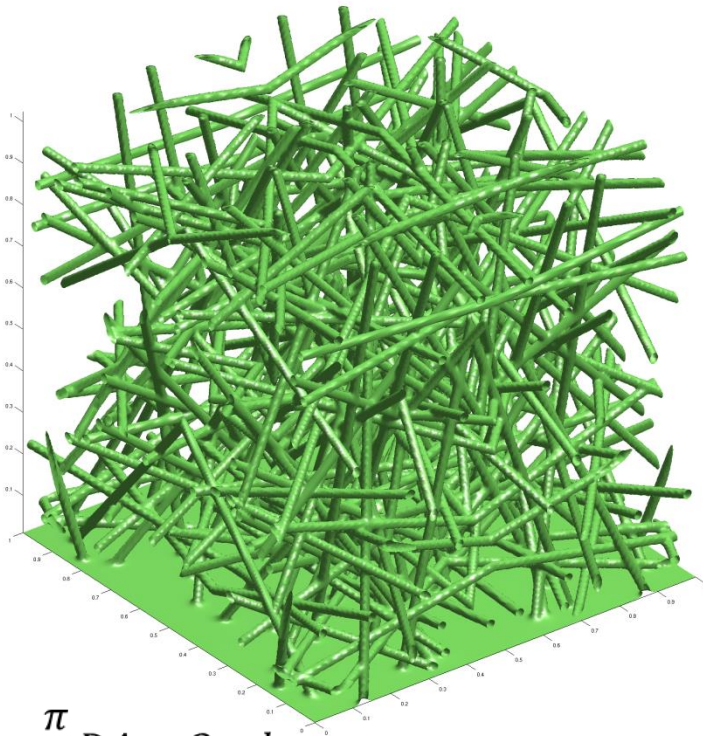
Discrepancy is due to tertiary and higher-order electrons.

**Velvet is well-suited to suppressing normally incident primary electrons**



# Simulations and Theory of SEY of complex surfaces: Fuzz/foam

Fuzz/foam: irregular lattice of isotropically-oriented fibers



$$u = \frac{\pi}{2}DA = 2rnh$$

$u$  dimensionless parameter,  $D$  area packing fraction,  $A$  aspect ratio of fibers,  $r$  radius of fibers,  $n$  area density of fibers,  $h$  height of fiber layer

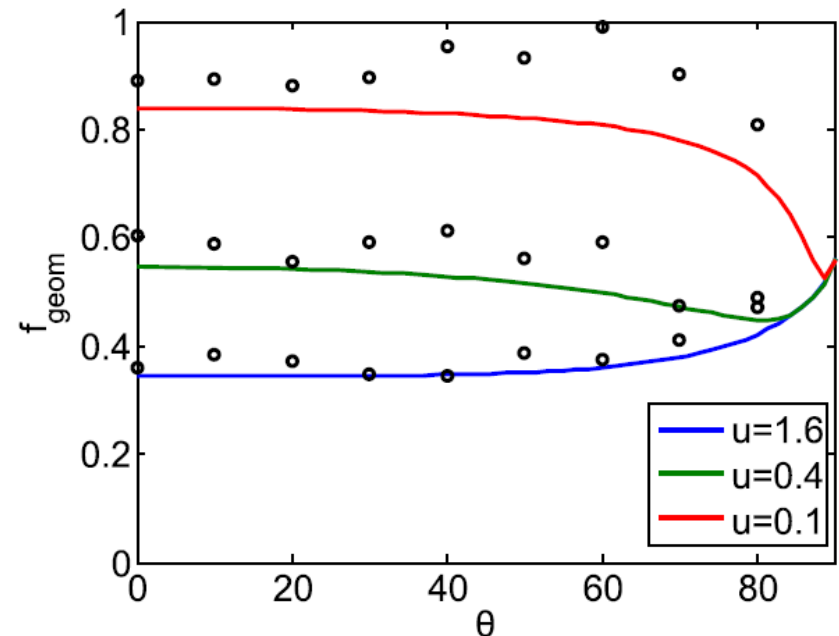
**SEY as a function of incident angle for different packing density of foam.**

Lines: Analytic model.

Points: Monte-Carlo simulations.

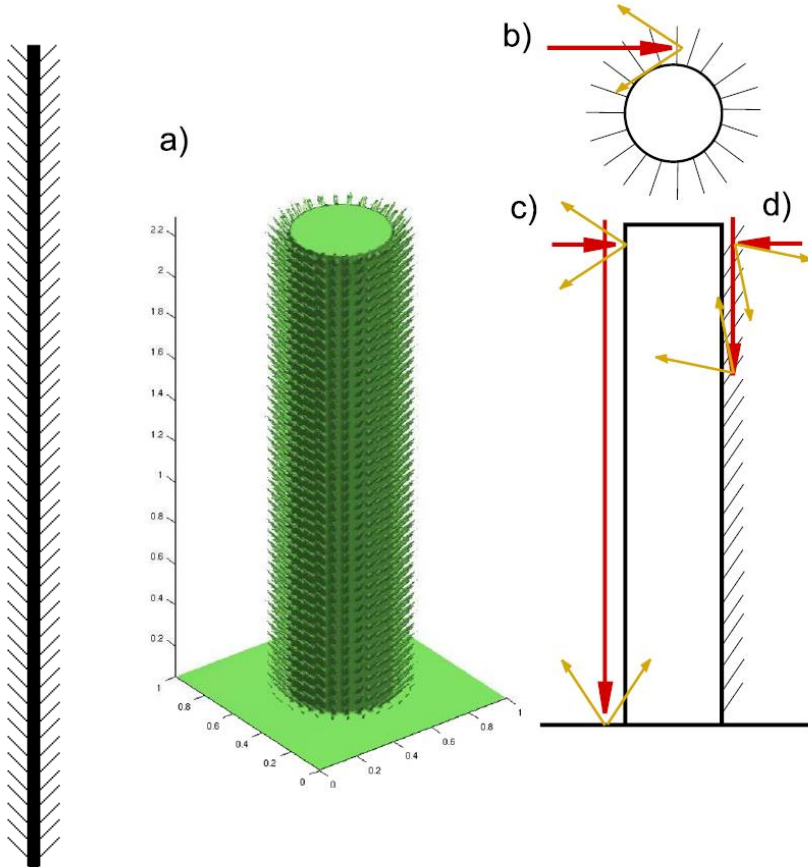
Discrepancy is due to tertiary and higher-order electrons.

**Foam is not well-suited to suppressing normally incident primary electrons**

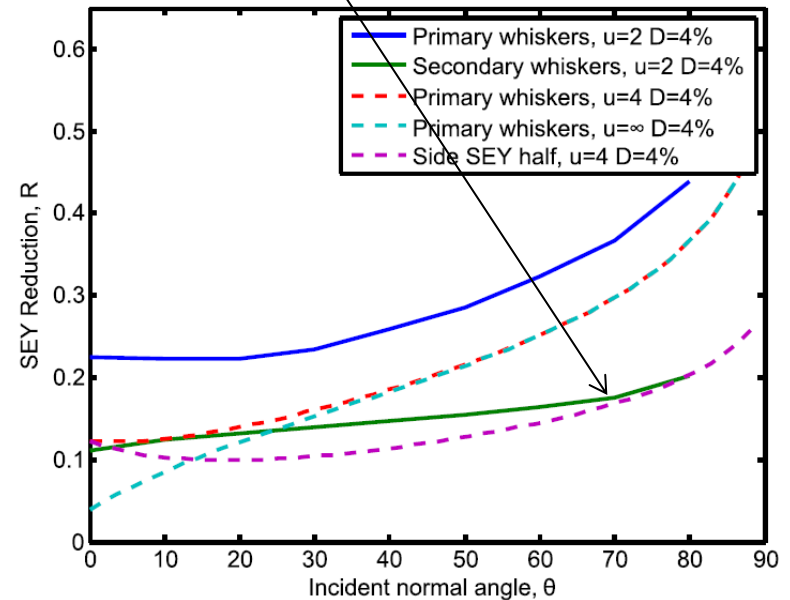


# Simulations and Theory of SEY of complex surfaces: Feathers

Feather: lattice of normally-oriented fibers with smaller, secondary fibers on the sides of that fiber.



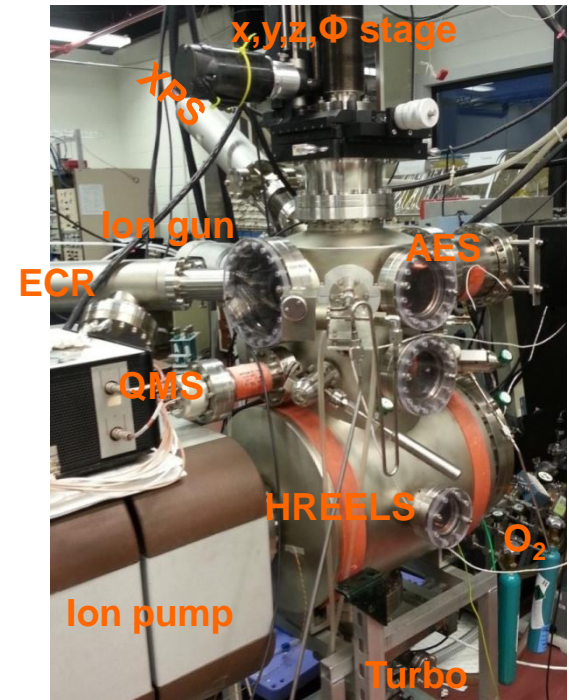
SEY as a function of incident angle for different packing density of foam. Feathers are able to suppress SEE for all electrons  $\sim 1/4$ .



C. Swanson and I. Kaganovich, J. Appl. Phys. (2017)

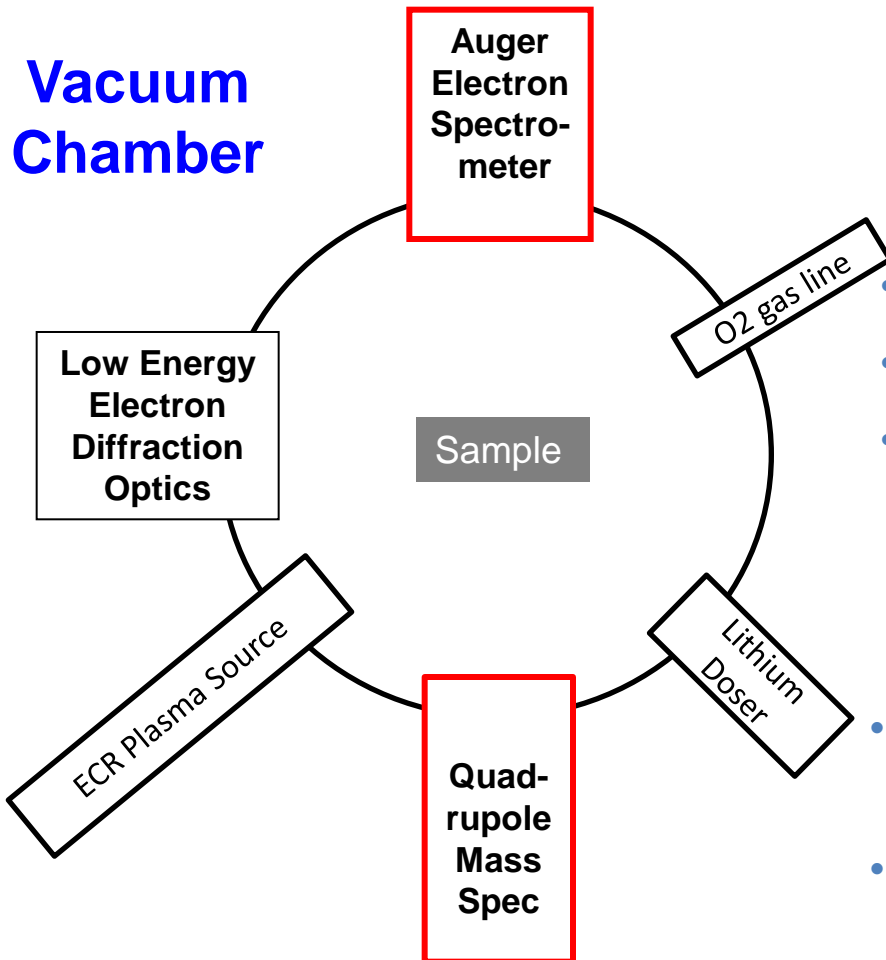
# PPPL experimental setup for SEE measurements

- $10^{-8}$  -  $10^{-10}$  Torr (turbo, ion, & Ti sublimation pumps)
- Quadrupole Mass Spectrometer
  - Background gas, temperature program desorption (TPD)
- Kimball Physics Pulsed Electron Source
  - SEE measurements of dielectric and conductive materials
- Auger Electron Spectroscopy (AES)
  - Sample composition, SEE
- Low Energy Electron Diffraction (LEED)/AES
  - SEE yield, angular dependence and energy distribution of SEE electrons
- Electron Cyclotron Resonance Plasma Source
  - Sample cleaning
- Resistive heating ( $\sim 1400\text{K}$  max)
  - Sample cleaning & conditioning, TPD
- $\text{LN}_2$  cooling ( $< 200\text{K}$ )
- High Resolution Electron Energy Loss Spectroscopy
- X-ray Photoelectron Spectroscopy (XPS)

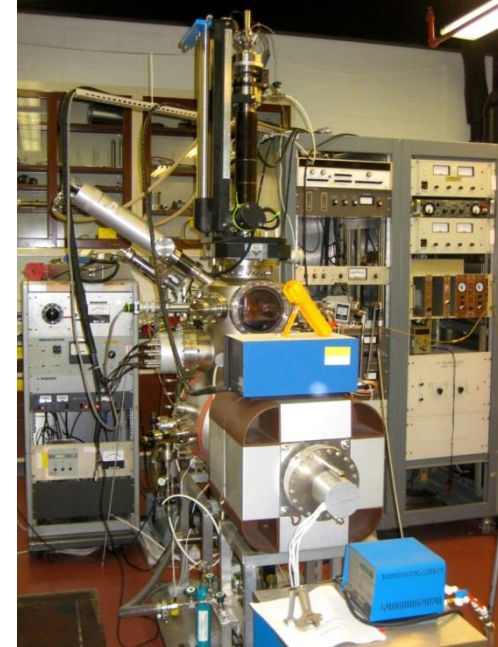


# PU experimental setup incorporates *in situ* analysis of material composition

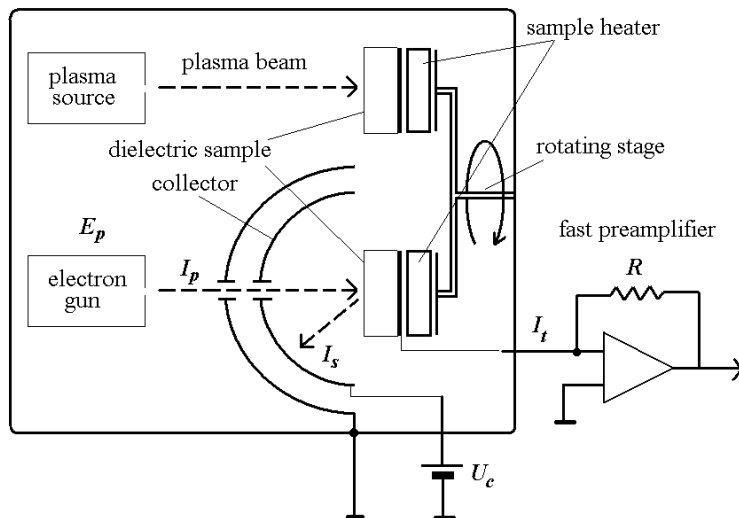
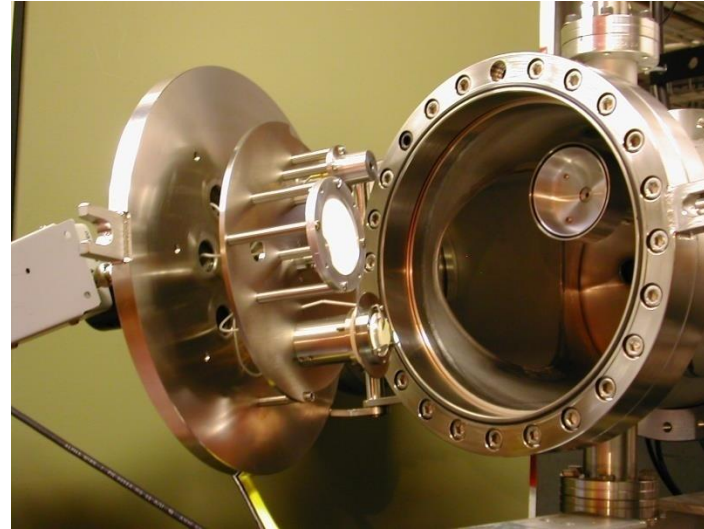
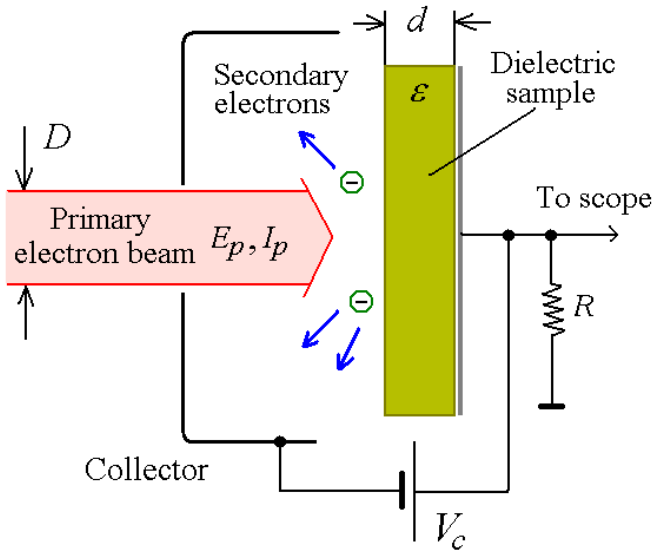
## Vacuum Chamber



- $P=2 \times 10^{-10}$  Torr
- Ni(110) substrate
- 40 ML (10 nm) of lithium on surface
- Can expose to  $O_2$  &  $H_2O$  to adjust composition
- Measure composition with Auger electron spectroscopy



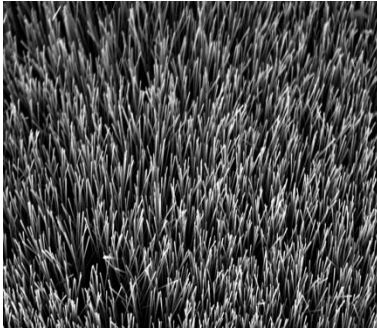
# Upgraded setup for measurements of SEE yield from micro-engineered materials



- Cryogenic system to maintain better vacuum ( $<10^{-8}$  torr) during SEE measurements
- Ion source to remove surface charges
- The upgrade allows to minimize, outgassing, surface, contamination, etc.

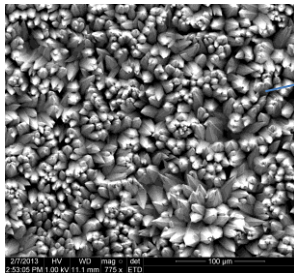
# SEY of surface micro-architected engineered materials to suppress SEE

Carbon velvet

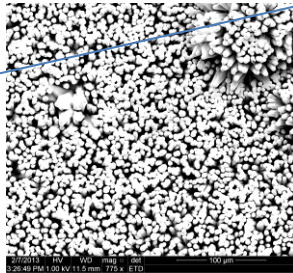


Dendrites

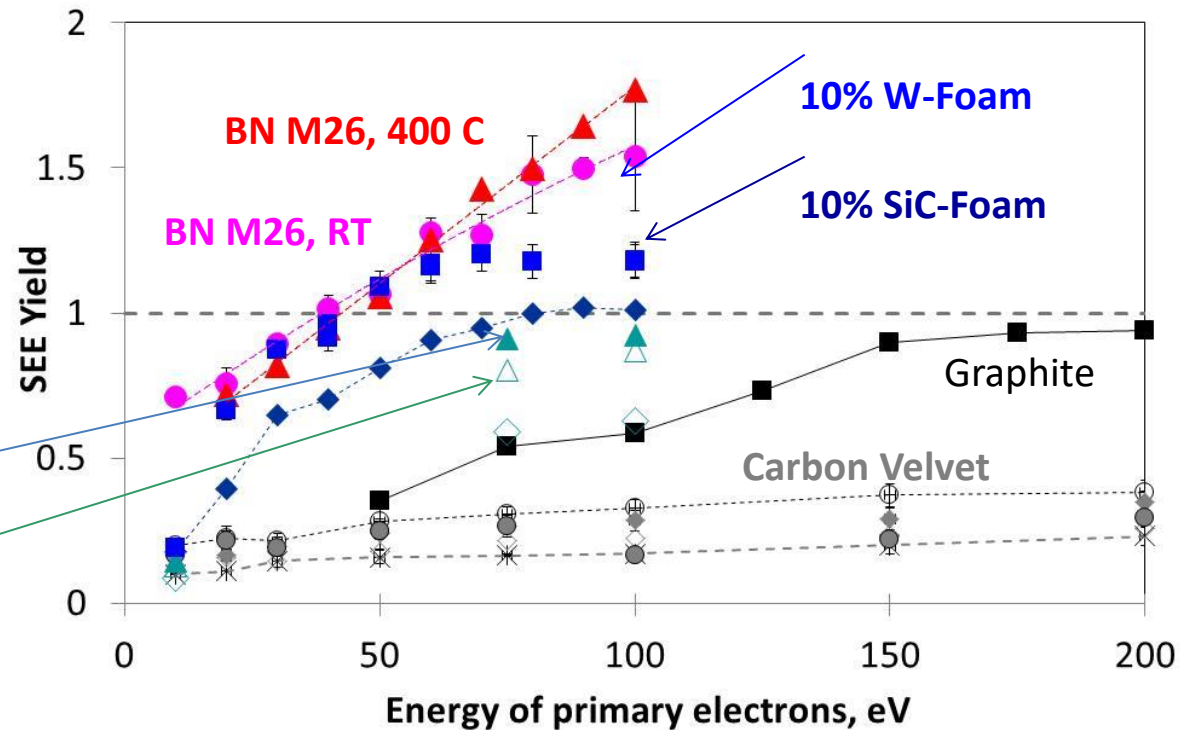
Mo-coated Re



W-coated Re

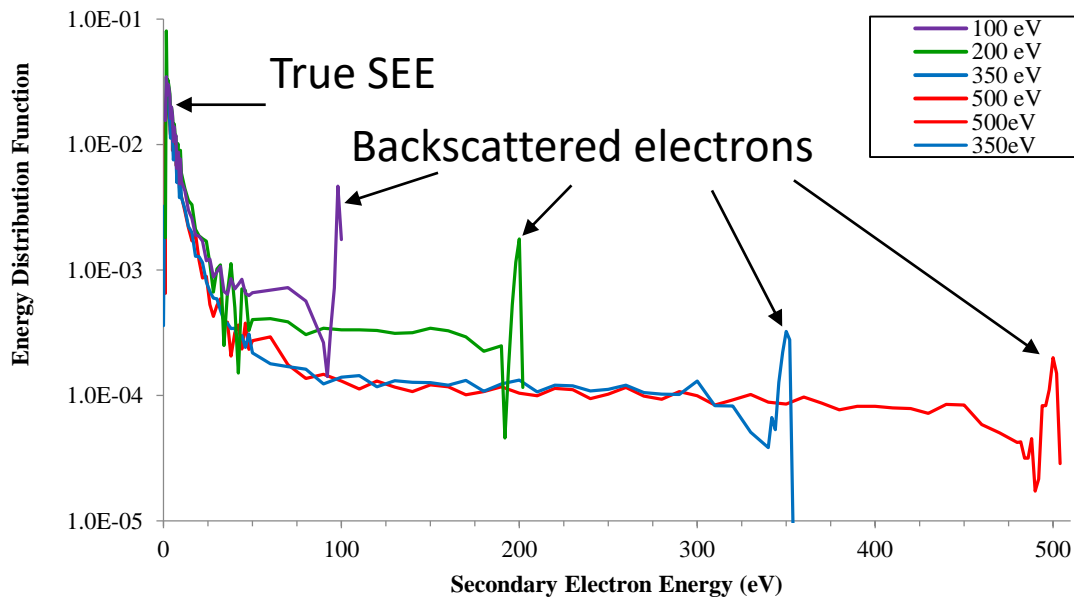


- Measured total SEE yield from velvets and dendrites:

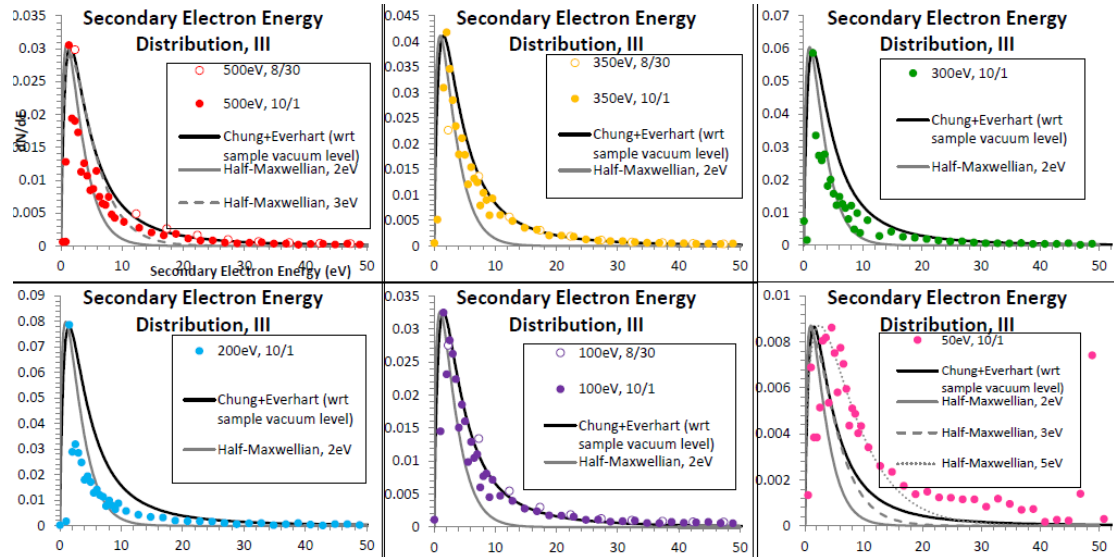


- Surface-architected materials can reduce the effective SEE yield by trapping SEE electrons between surface architectural features.
- The SEE reduction is more significant for high aspect ratio ( $1:10^3$ ) velvets than for low aspect ratio ( $1:10$ ) dendritic coatings.

# EEDF of SEE Electrons from Graphite



Measured electron energy distribution function (EEDF) for true SEE – important input for plasma-wall interaction.



# SEE yield for W- flat samples

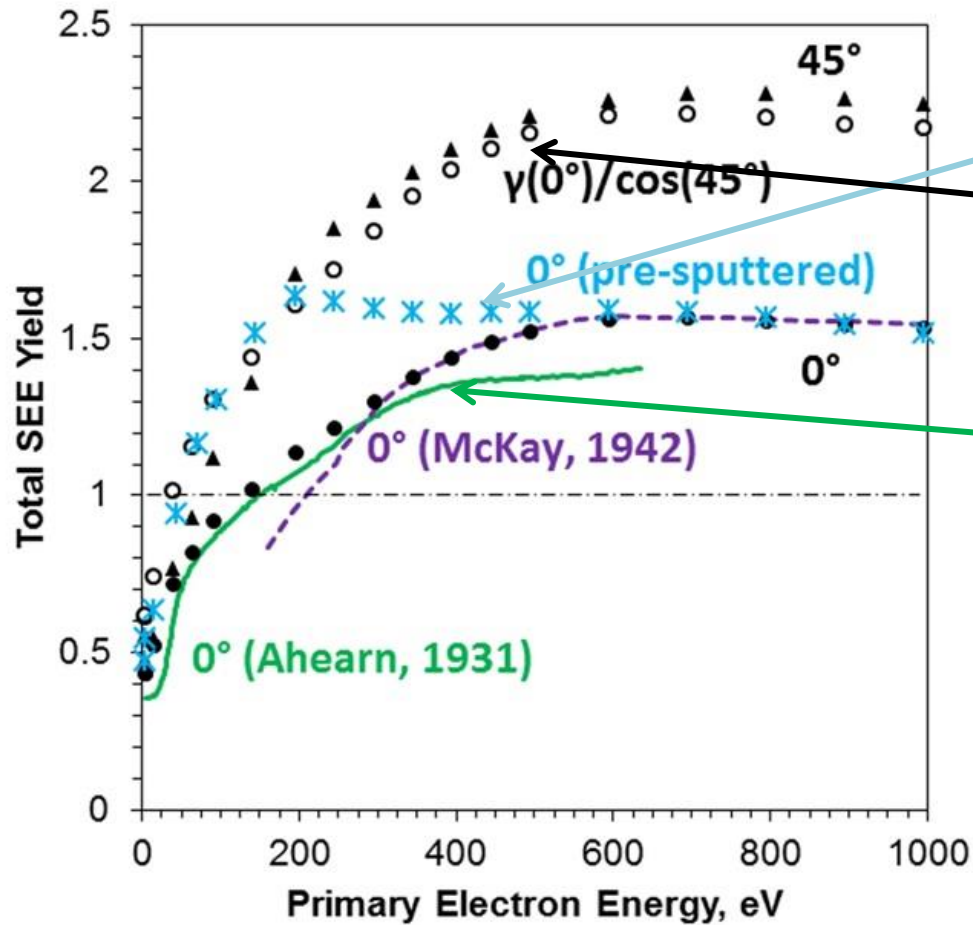


*Fig.* Total SEE yield of smooth pre-sputtered (blue asterisks) and post-sputtered (black filled circles/triangles) W at 0° and 45°.

SEE from post-sputtered W at 0° matches previous results of cleaned W (green and purple lines), and at 45° follows a  $1/\cos(\theta)$  dependence (black unfilled circles).

SEE from pre-sputtered W is higher than from post-sputtered W since C, O, and many oxides increase SEE.

# SEE yield for W-fuzz and W- flat samples

## Angular dependence of SEE yield

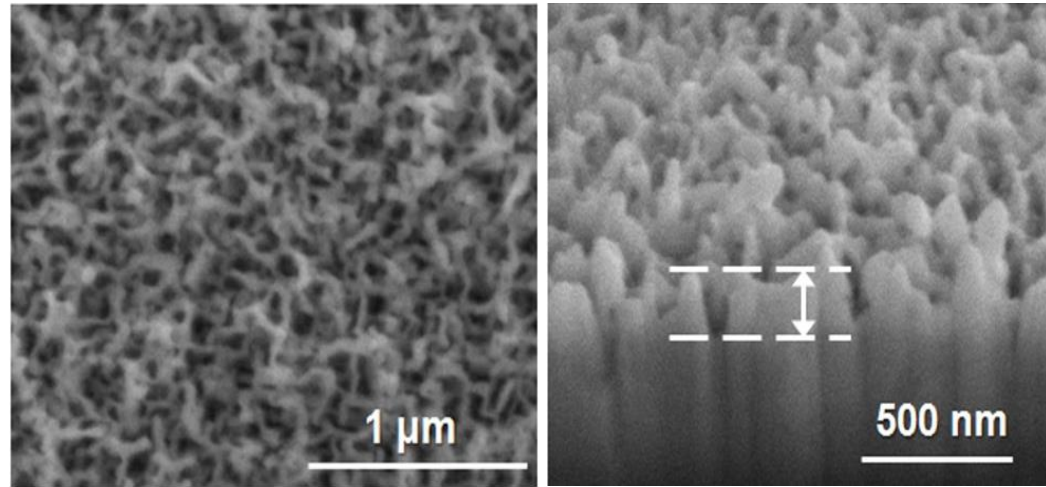
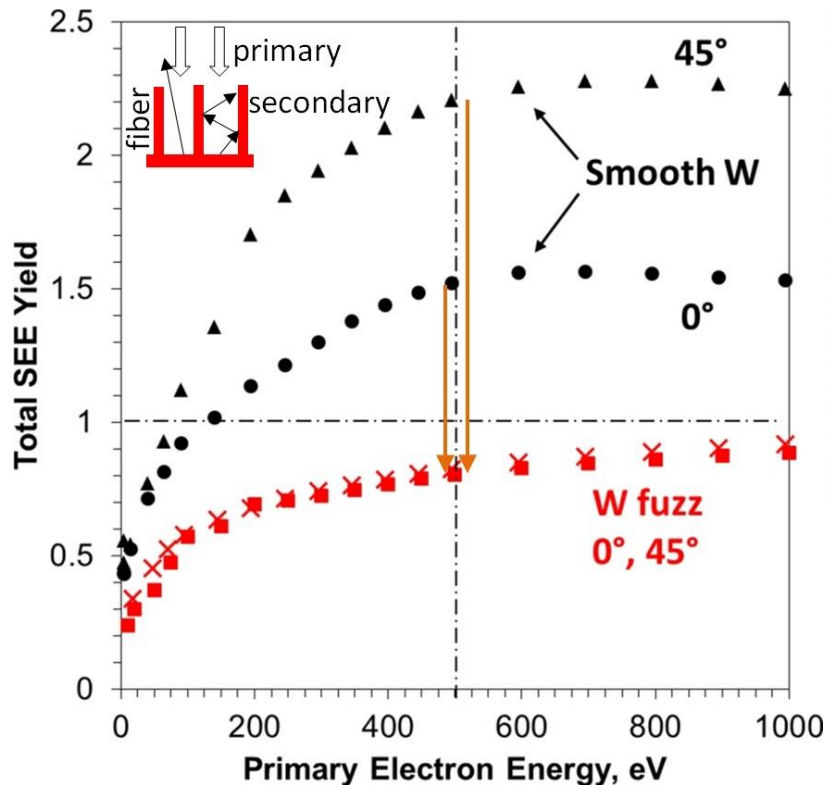
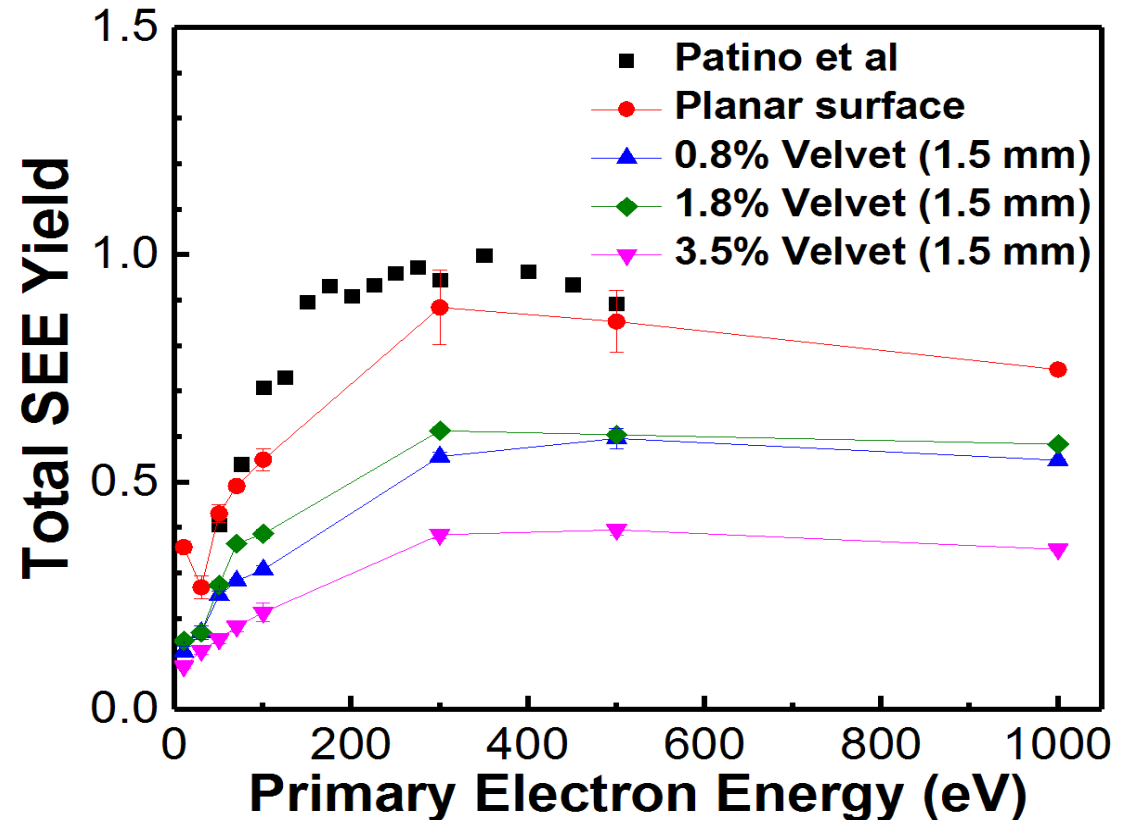
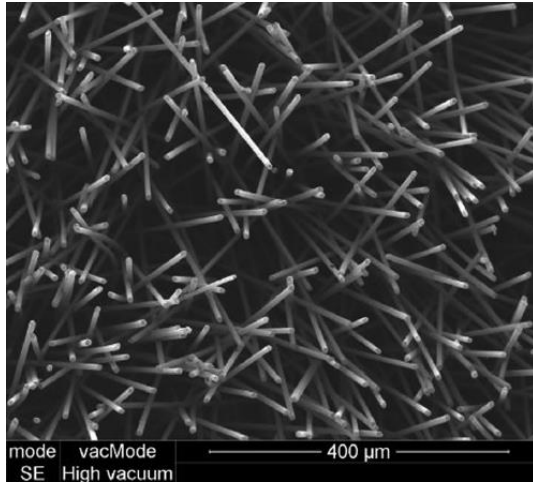


*Fig:* SEM image of (top) top view and (bottom) side view of W fuzz formed when exposed to He plasma at elevated temperatures (i.e., 60 eV He<sup>+</sup>, flux =  $3.7 \times 10^{21} \text{ m}^{-2} \text{ s}^{-1}$ , fluence =  $1.3 \times 10^{25} \text{ m}^{-2}$ , sample at 1270 K). Fibers are 25-50 nm in diameter and 100-200 nm long.

*Fig:* Total SEE yield from W fuzz at 0° and 45° (red squares/crosses) compared to smooth post-sputtered W (black circles/triangles). **SEE from W fuzz is >40% lower than from smooth W** (despite W fuzz having more C, O, oxidation) due to trapping of secondary electrons within the fuzz. **SEE from W fuzz is independent of primary electron incident angle** since the orientation of fibers leads to a wide distribution of local incident angles.

# Velvet: surface-architected material with low SEE

- Total SEE yield at normal incidence measured in vacuum

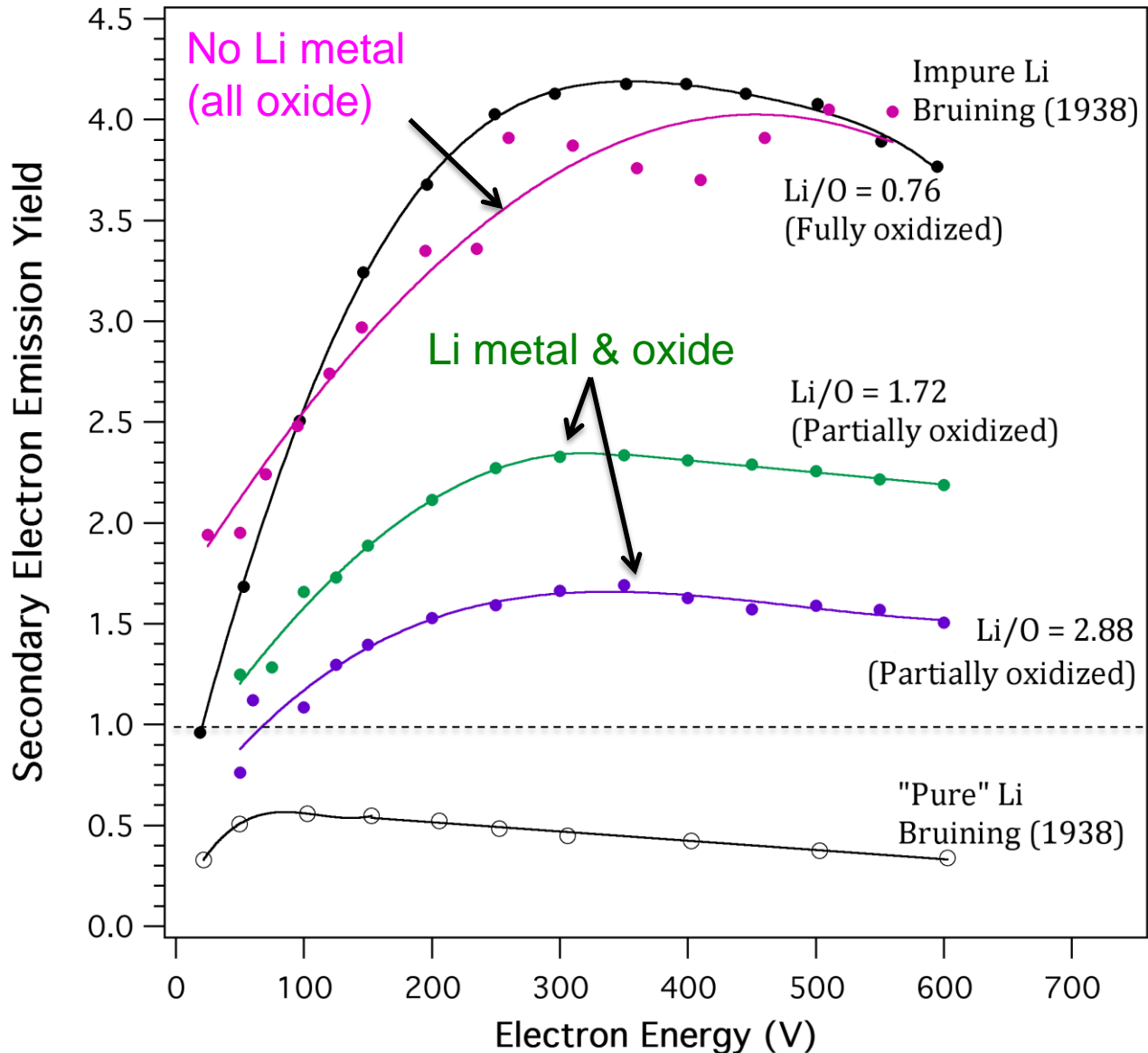


- SEE from velvet can be several times lower than SEE from carbon.

# SEE Yield of Li & LiO<sub>x</sub>

As oxygen content **increases**, SEY greatly increased.

A. M. Capece, M. I. Patino, Y. Raitzes, and B. E. Koel, Applied Physics Letters **109**, 011605 (2016)

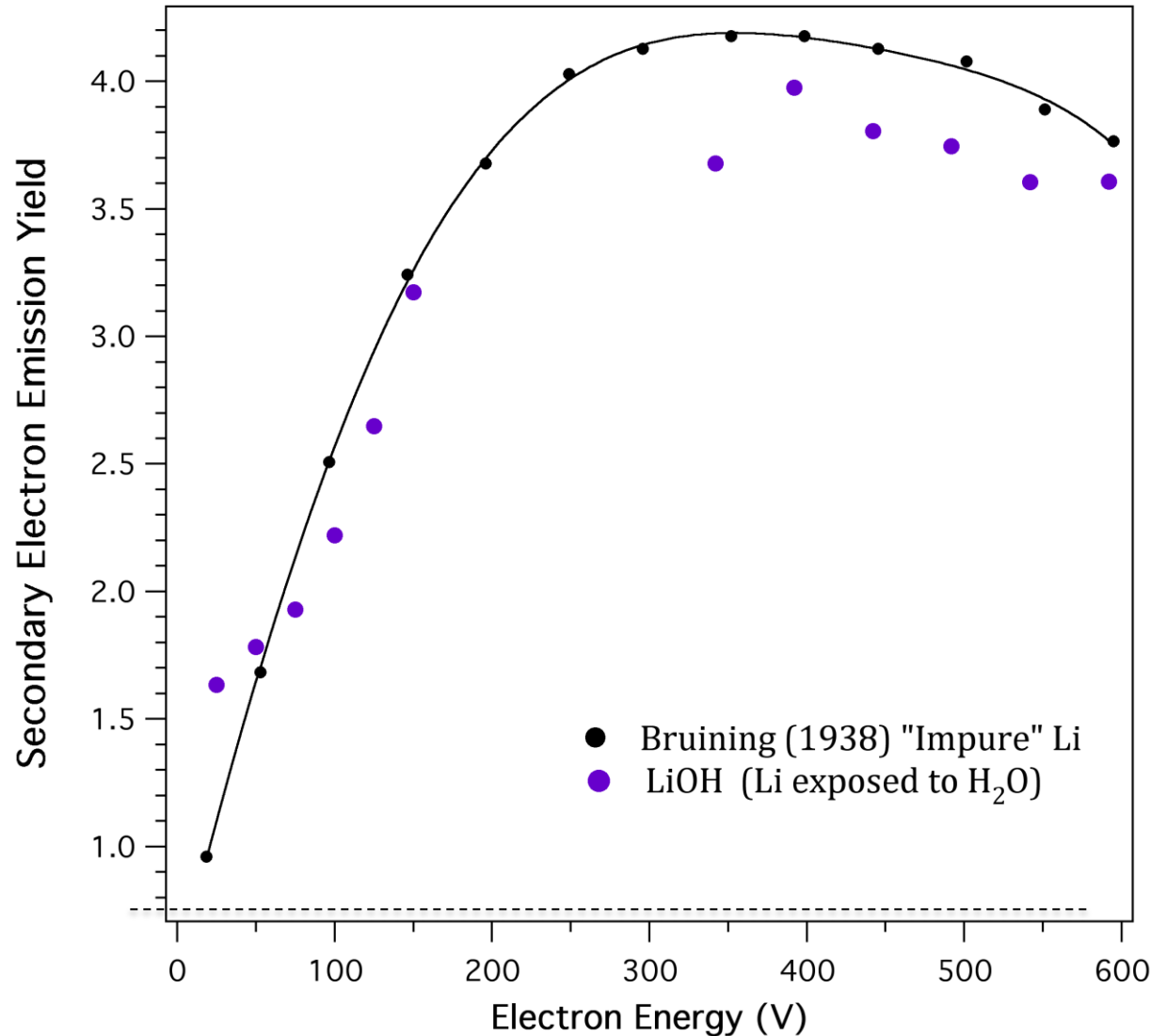


# SEE Yield of LiOH

Water is major contaminant in vacuum systems and gives yields similar to fully oxidized lithium.

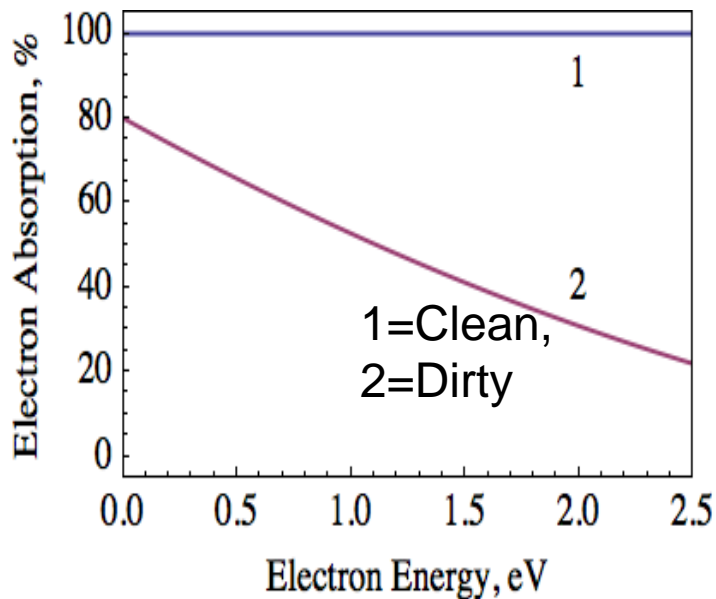
Yield of LiOH similar to oxidized Li

Applied Physics Letters  
109, 011605 (2016)



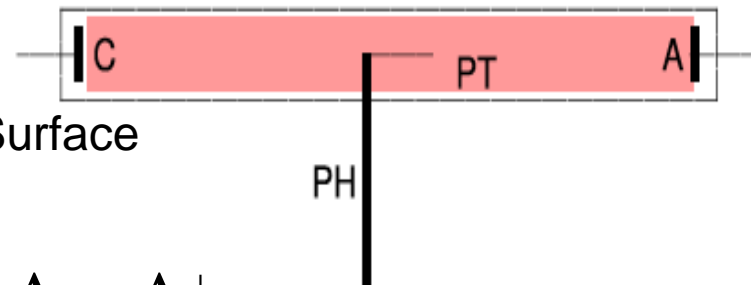
# SEY was measured **within few eV precision** using a wall probe using penning produced electrons with a specific energy

A metallic boundary reflects a *negligible amount* of low-energy incident electrons when uncontaminated (“clean”) and reflects a significant amount when contaminated by monolayers of adsorbent.

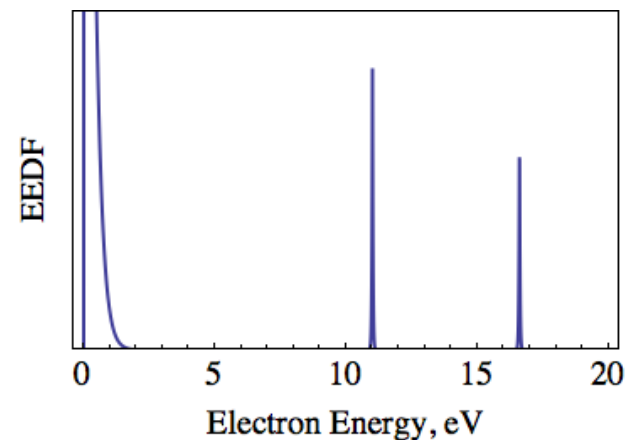


Neon Plasma

Molybdenum Surface



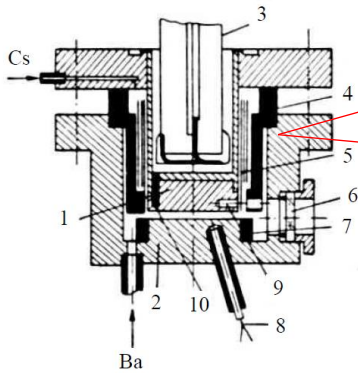
Penning ionization gives electrons of fixed energy.



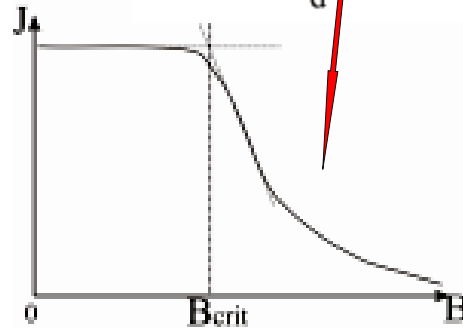
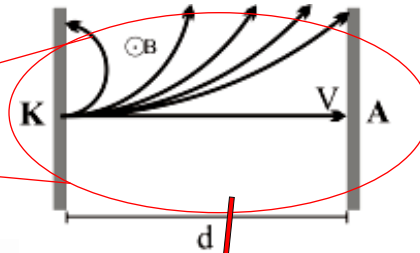
Demidov et al., Phys. Plasmas **22**, 104501 (2015)

# SEY was measured **within few eV precision** using a weak magnetic field in thermoemitting device

**Knudsen Cs-Ba plasma diode with surface ionisation**



**Electron trajectories in magnetic field**



**Dependence of anode current on magnetic field**

**Experimental results for reflection coefficient and effective work function for different surfaces**

$r_{hkl}$	$r_0$	$\Phi_{exp}$
110	0.3	5.3
112	0.25	4.8
100	0.15	4.7
111	0.1	4.4
116	0.05	4.3
Poly-crystal	0.15	4.6

It is shown that for poly-crystal surfaces, the SEE yield can be indeed very high ( $\sim 0.8$ ) but still not approaching unity. This result is explained by additional reflection of primary electrons from a potential barrier near the poly-crystal surface. The contribution of electron reflection from the potential barrier and the surface has been indented and studied.

# Conclusions

---

- **Derived analytical formulas for Secondary Electron Emission Yield for complex surfaces: velvet, foam/fuzz, feathers and verified with a MC code.**

**Feathered surfaces are best at reducing SEY by a factor of 4.**

- **PPPL has sophisticated experimental set ups to measure SEY in cleaned and oxidized samples, including dielectrics.**

**Measured SEY for several surface micro-structured engineered materials to suppress SEE: velvet, fuzz, dendritic coatings.**

**High-aspect-ratio velvet reduces SEY most compared to low-aspect-ratio dendritic coatings.**

**Measured EEDFs of true secondaries at low energies.**

**Measured angular dependence on primary electrons of SEY for W and fuzz.**

**Measured effect of oxidation on SEY of W, W fuzz and Li.**

**Measured SEY of very low energy using penning reaction in plasma magnetized thermionic discharge.**

# PPPL Relevant References

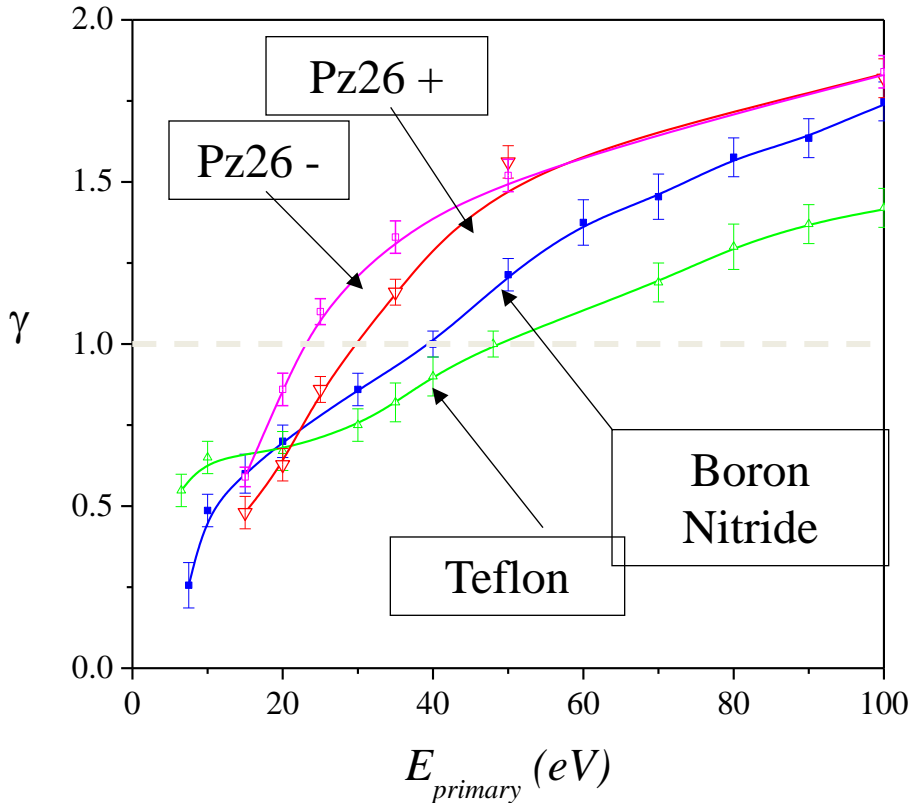
---

- **Secondary electron emission yield from high aspect ratio surfaces**, Chenggang Jin, Angelica Ottaviano and Yevgeny Raitses, Journal of Applied Physics 122, 173301 (2017)
- **"Feathered" fractal surfaces to minimize secondary electron emission for a wide range of incident angles**, Charles Swanson and Igor D. Kaganovich, Journal of Applied Physics 122, 043301 (2017)
- **Modeling of reduced effective secondary electron emission yield from a velvet surface**, C. Swanson, I. D Kaganovich, Journal of Applied Physics 120, 213302 (2016)
- **Secondary electron emission from a plasma-generated nanostructure tungsten fuzz**, M. Patino, Y. Raitses and R. Wirz, Applied Physics Letters 109, 201602 (2016)
- **Secondary electron emission from lithium and lithium compounds**, A.M. Capece, M.I. Patino, Y. Raitses and B. E. Koel Applied Physics Letters 109, 0011605 (2016)
- **Analysis of secondary electron emission for conducting materials using 4-grid LEED/AES optics**, M. I. Patino, Y. Raitses, B. E. Koel and R. E. Wirz, Journal of Physics D: Applied Physics 48, 195204 (2015)
- **Effect of Secondary Electron Emission on Electron Cross-Field Current in ExB Discharges**, Y. Raitses, I. D. Kaganovich, A. Khrabrov, D. Sydorenko, N. J. Fisch, A. Smolyakov, IEEE Transactions on Plasma Science 39, 995 (2011).
- **Measurements of secondary electron emission effects in Hall thrusters**, Y. Raitses, A. Smirnov, D. Staack, and N. J. Fisch, Physics of Plasmas 13, 014502 (2006).
- **Kinetic simulation of secondary electron emission effects in Hall thrusters**, D. Sydorenko, A. Smolyakov, I. Kaganovich, and Y. Raitses, Physics of Plasmas 13, 014501 (2006).
- **Yield of Secondary Electron Emission from Ceramic Materials of Hall Thruster**, A. Dunavesky, Y. Raitses and N. J. Fisch, Physics of Plasmas, 10, 2574 (2003).

## Relevant Bibliography

- [1] J. Scholtz et al., "Secondary electron emission properties," *Philips J. Res.* 50, 375 (1996).
- [2] Sydorenko, Dmytro. "Particle-in-Cell Simulations of Electron Dynamics in Low Pressure Discharges with Magnetic Fields," 2006. <https://ecommons.usask.ca/handle/10388/etd-06142006-111353>.
- [3] Vtorichnaya Elektronnaya Emissiya, edited by I. M. Bronstein and B. S. Fraiman (Nauka, Movkva, 1969), p. 340 (in Russian).
- [4] Campanell, M. D., A. V. Khrabrov, and I. D. Kaganovich. "Absence of Debye Sheaths Due to Secondary Electron Emission." *Physical Review Letters* 108, no. 25 (June 18, 2012): 255001.
- [5] Kushner, M. J. "Mechanisms for Power Deposition in Ar/SiH<sub>4</sub> Capacitively Coupled RF Discharges." *IEEE Transactions on Plasma Science* 14, no. 2 (April 1986): 188–96. <https://doi.org/10.1109/TPS.1986.4316522>.
- [6] J. R. M. Vaughan, "Multipactor," *IEEE Trans. Electron Devices* 35, 1172–1180 (1988).
- [7] I. Kaganovich, Y. Raitses, D. Sydorenko, and A. Smolyakov, "Kinetic effects in a Hall thruster discharge," *Phys. Plasmas*, vol. 14, no. 5, p. 057104, May 2007.
- [8] Zimmermann, Frank. "A Simulation Study of Electron Cloud Instability and Beam Induced Multipacting in the LHC," 1997.
- [9] M. T. F. Pivi et al., "Sharp reduction of the secondary electron emission yield from grooved surfaces," *J. Appl. Phys.* 104, 104904 (2008).
- [10] V. Baglin, J. Bojko, O. Grabner, B. Henrist, N. Hilleret, C. Scheuerlein, and M. Taborelli, "The secondary electron yield of technical materials and its variation with surface treatments," in *Proceedings of EPAC 2000*, 26–30 June 2000, Austria Center, Vienna, pp. 217–221.
- [11] M. Ye, W. Dan, and H. Yongning, "Mechanism of total electron emission yield reduction using a micro-porous surface," *J. Appl. Phys.* 121(12), 124901 (2017).
- [12] J. Vaughan, "A new formula for secondary emission yield," *IEEE Trans. Electron Devices* 36, 1963 (1989).
- [13] M. Patino, Y. Raitses, B. Koel, and R. Wirz, "Application of Auger spectroscopy for measurement of secondary electron emission from conducting material for electric propulsion devices," in *33rd International Electric Propulsion Conference (IPEC)*, The George Washington University, Washington, DC, USA, 6–10 October 2013.
- [14] Swanson, Charles, and Igor D. Kaganovich. "Modeling of Reduced Effective Secondary Electron Emission Yield from a Velvet Surface." *Journal of Applied Physics* 120, no. 21 (December 7, 2016): 213302. <https://doi.org/10.1063/1.4971337>.
- [15] Jin, Chenggang, Angelica Ottaviano, and Yevgeny Raitses. "Secondary Electron Emission Yield from High Aspect Ratio Carbon Velvet Surfaces." *Journal of Applied Physics* 122, no. 17 (November 1, 2017): 173301. <https://doi.org/10.1063/1.4993979>.
- [16] Swanson, Charles, and Igor D. Kaganovich. "'Feathered' Fractal Surfaces to Minimize Secondary Electron Emission for a Wide Range of Incident Angles." *Journal of Applied Physics* 122, no. 4 (July 24, 2017): 043301. <https://doi.org/10.1063/1.4995535>.
- [17] Swanson, Charles, and Igor D. Kaganovich. "Modeling of Reduced Secondary Electron Emission Yield from a Foam or Fuzz Surface." *Journal of Applied Physics* 123, no. 2 (January 10, 2018): 023302. <https://doi.org/10.1063/1.5008261>.
- [18] Wang, Kun, R. P. Doerner, M. J. Baldwin, F. W. Meyer, M. E. Bannister, Amith Darbal, Robert Stroud, and Chad M. Parish. "Morphologies of Tungsten Nanotendrils Grown under Helium Exposure." *Scientific Reports* 7 (February 14, 2017): 42315. <https://doi.org/10.1038/srep42315>.
- [19] M. Patino, Y. Raitses, and R. Wirz, "Secondary electron emission from plasma-generated nanostructured tungsten fuzz," *Appl. Phys. Lett.* **109**(20), 201602 (2016). <https://doi.org/10.1063/1.4967830>
- [20] Gunn J P 2012 *Plasma Phys. Control. Fusion* **54** 085007
- [21] Ramos, Manuel, Félix Galindo-Hernández, Ilke Arslan, Toby Sanders, and José Manuel Domínguez. "Electron Tomography and Fractal Aspects of MoS<sub>2</sub> and MoS<sub>2</sub>/Co Spheres." *Scientific Reports* 7, no. 1 (September 26, 2017): 12322. <https://doi.org/10.1038/s41598-017-12322-8>

# Secondary electron emission yield from dielectric materials

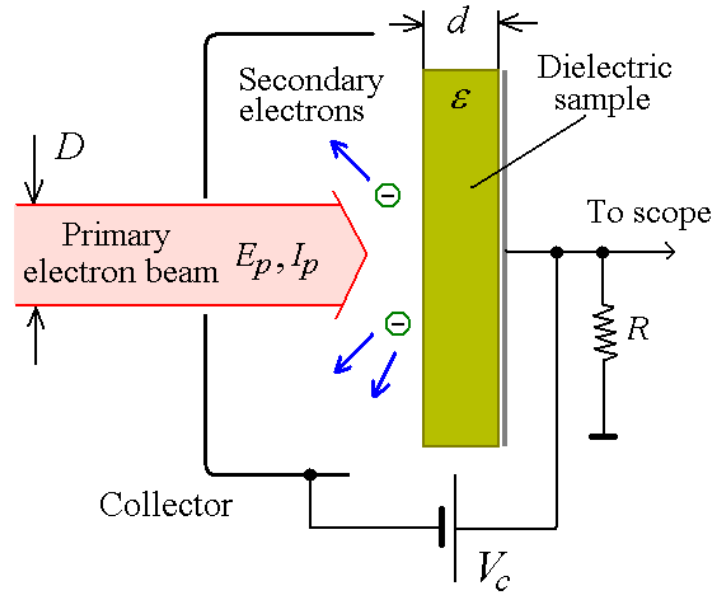


## Note:

for Boron Nitride ceramic, if plasma (primary) electrons have Maxwellian electron energy distribution (EEDF):

$$\chi(T_e) = 1 \text{ at } T_e = 18.3 \text{ eV}$$

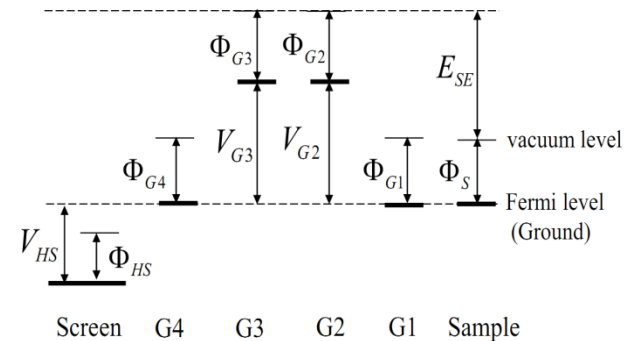
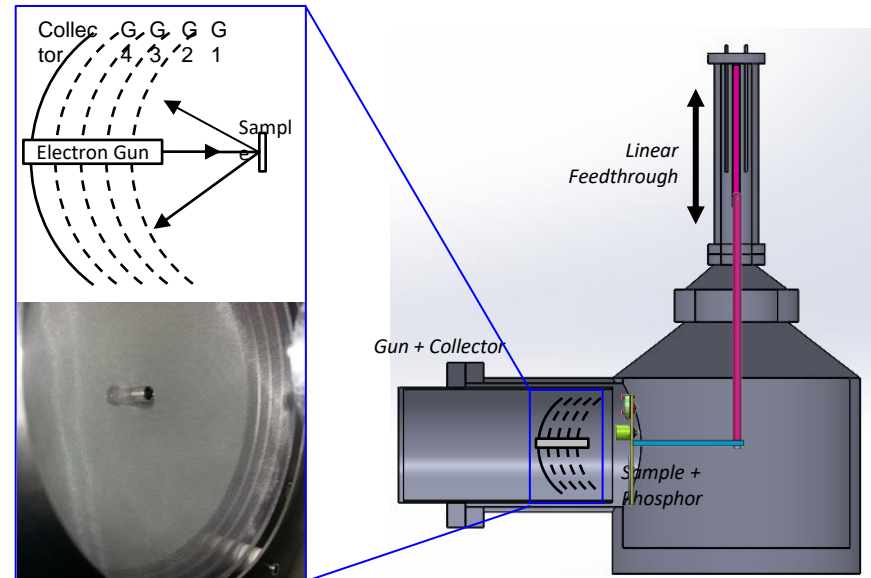
# “Sample” method to measure SEE yield from dielectric and high electric resistance materials



- Faraday cup to measure the primary electron current,  $I_p$
- Sample to ground current to measure the sample current,  $I_s$
- A slightly positively biased collector to attract SEE electrons
- SEE current is obtained from  $I_{SEE} = I_p - I_s$
- SEE yield is estimated as  $\gamma = I_{SEE} / I_p$

# Measurements of SEE Properties of Materials

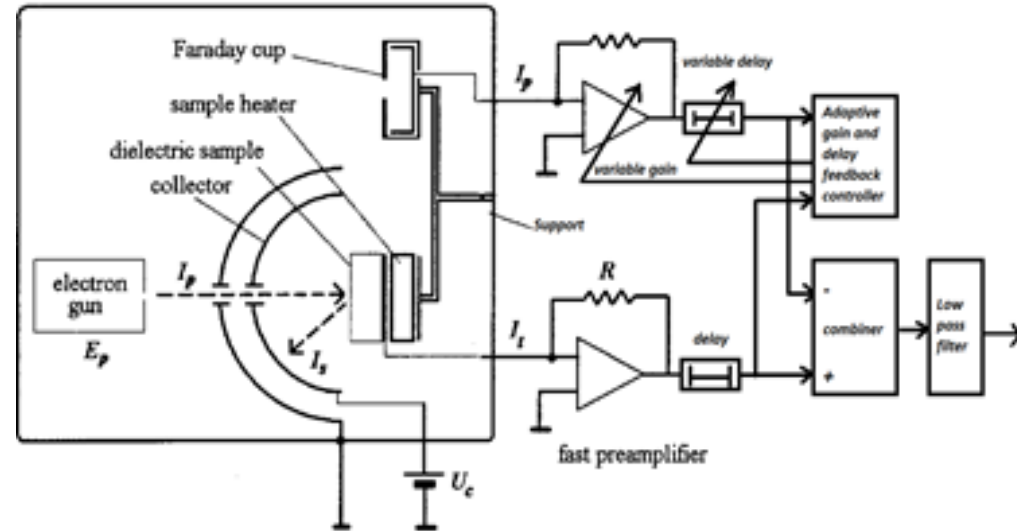
- **PPPL Electron LEED-Auger Spectroscopy System:**
  - UHV facility:  $1 \times 10^{-8}$  Torr.
  - Thermionic emission electron gun: 3-1600eV.
  - Retarding potential analyzer for measurements of EEDF of SEE electrons.
  - Conducting and dielectric materials.
- Use two measurement methods of the SEE yield:
  - i) biased sample
  - ii) biased collector



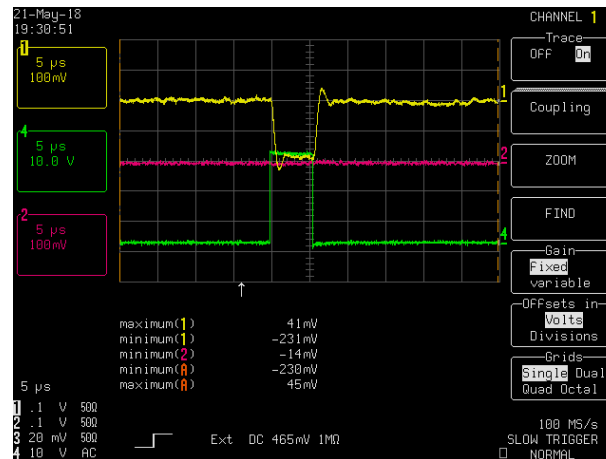
Energy level diagram for LEED/AES optics.

# High signal-to-noise measurements of SEE currents

- Fast amplifiers with bandwidth of 10 MHz, gain  $>10^7$  V/A (1 V for 100 nA) and the current resolution of  $<1$  nA.
- Reference method – Faraday cup signal is subtracted from the Sample signal to compensate for ambient noise during the pulse.
- Example of the measured sample current from 95%  $\text{Al}_2\text{O}_3$

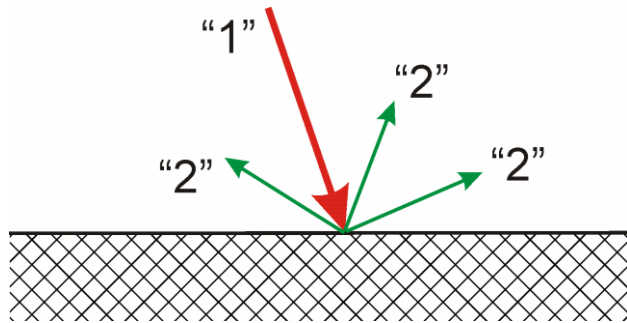


Primary energy: 300 eV  
 Sample current: 20 nA  
 Pulse:  $\sim 5 \mu\text{s}$   
 SEE yield:  $\gamma > 1$

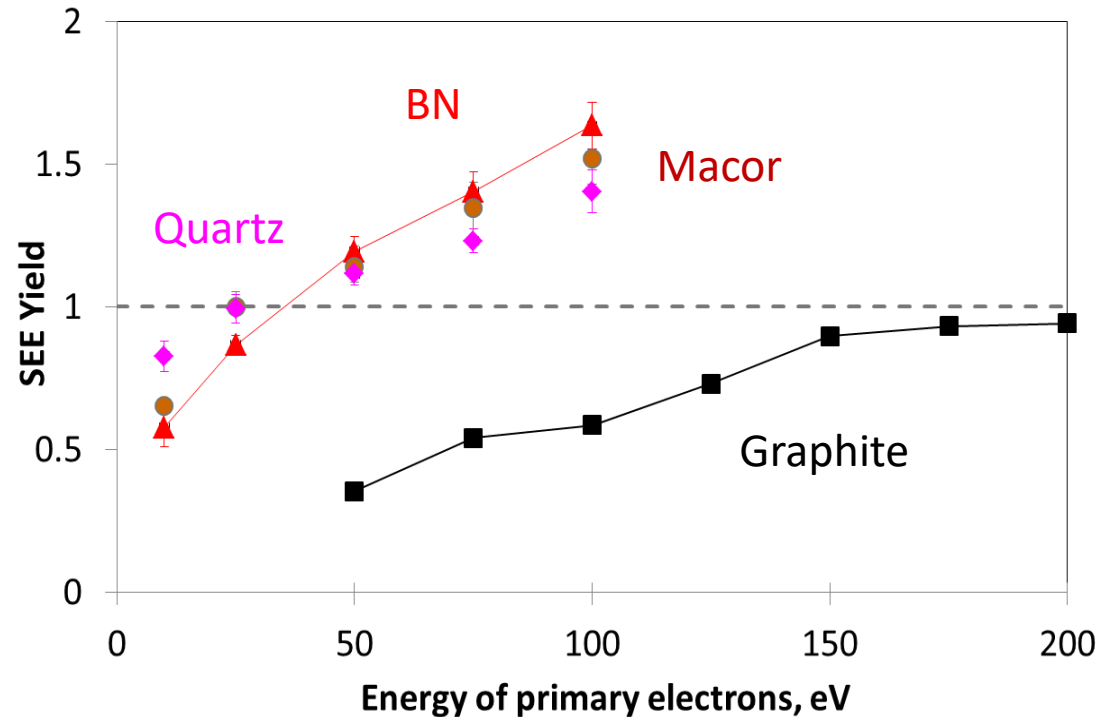


**Sample current signal**  
**Faraday cup signal**  
**Beam pulse waveform**

# SEE Properties of Ceramic Materials and Graphite



$$\gamma = \frac{\text{SEE}}{\text{Primaries}}$$



- Strong SEE effects on plasma-wall interaction occur when SEE approaches 1.
- For ceramic materials, SEE yield is higher and approaches 1 at lower energies than for metals due to a weaker scattering of SEE electrons on phonons (for insulators),  $\lambda \sim 20$  nm, than on electrons (for metals),  $\lambda \sim 1$  nm.

# Fuzz characterization

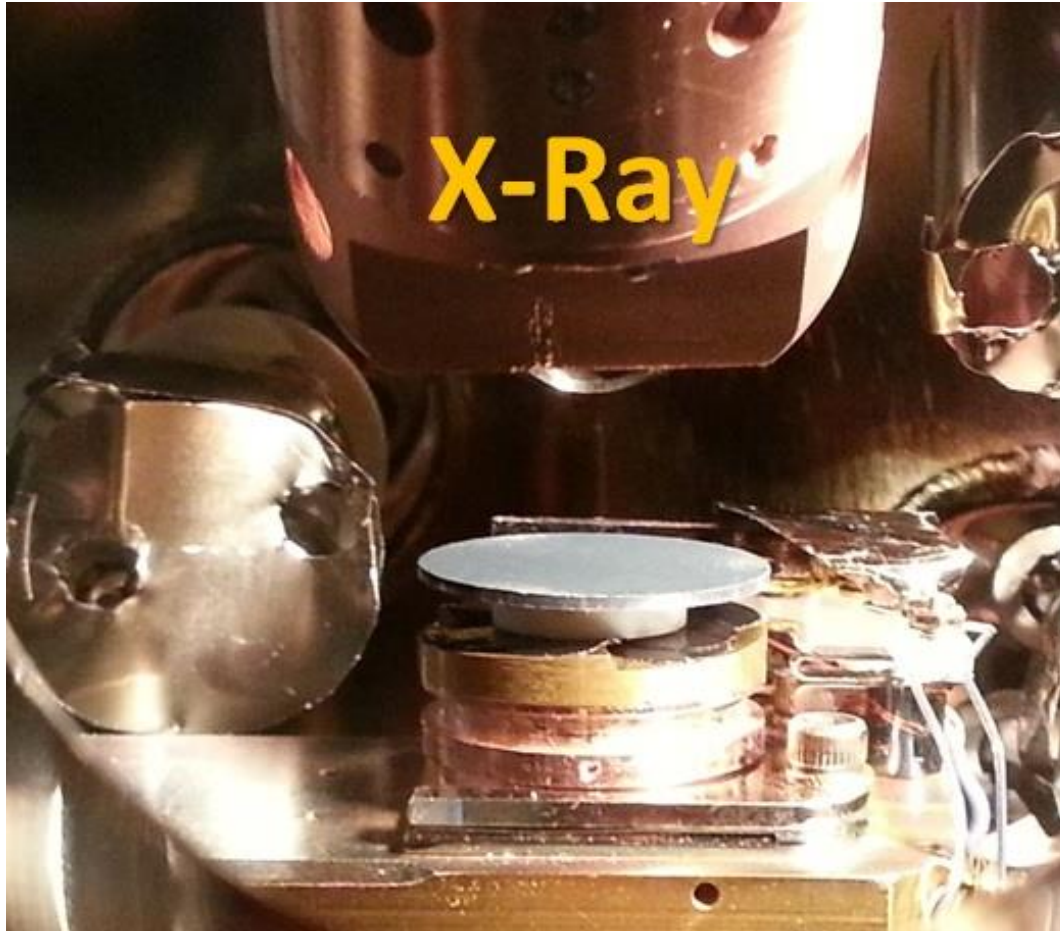


***Fig 6:*** Front view of the facility showing the W fuzz sample under the X-ray source.

# Fuzz chemical content

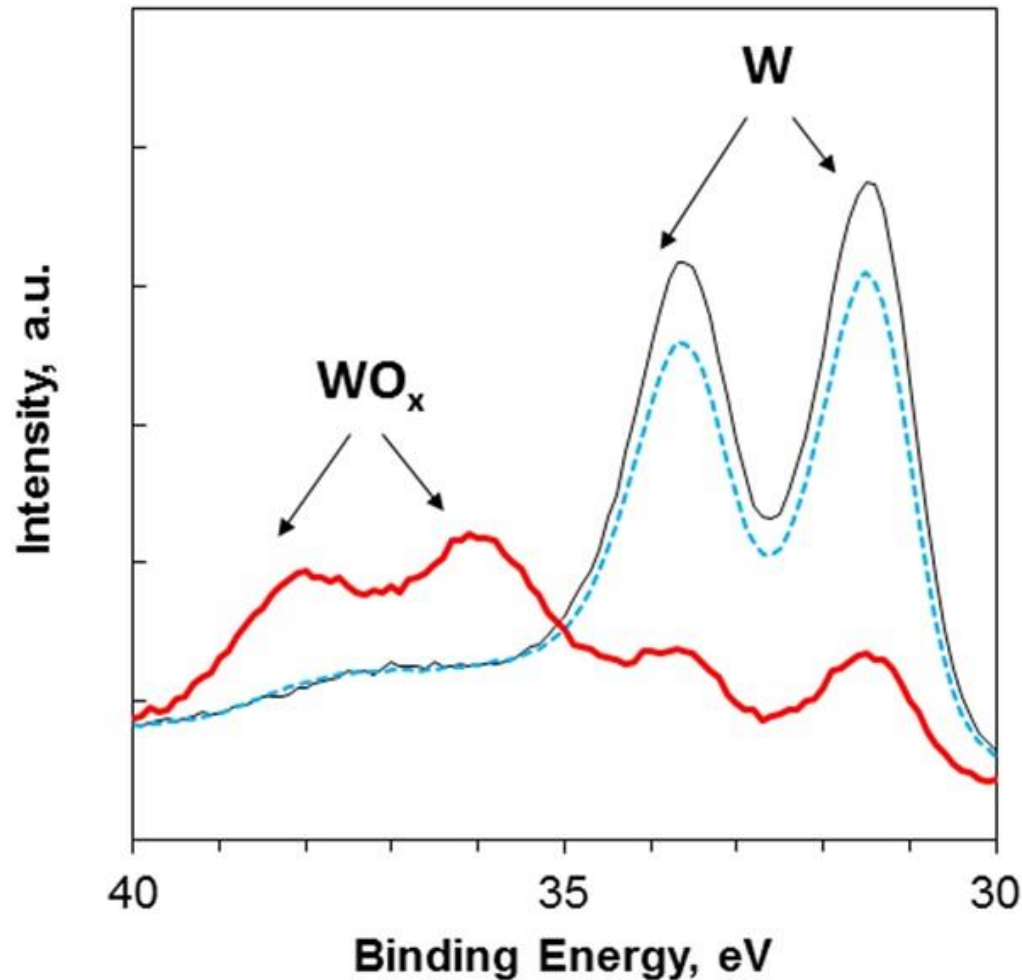
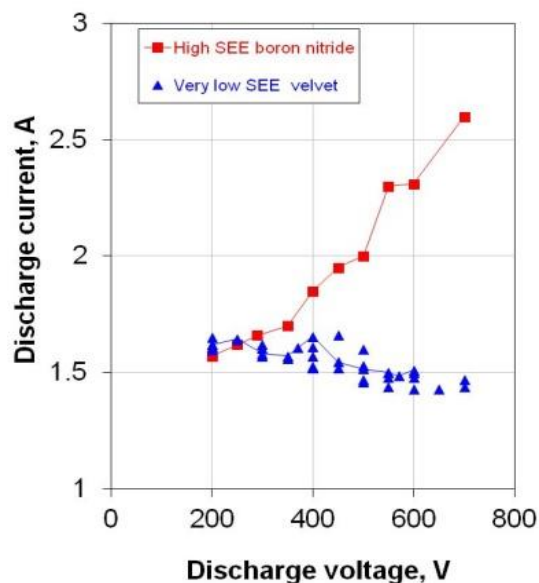
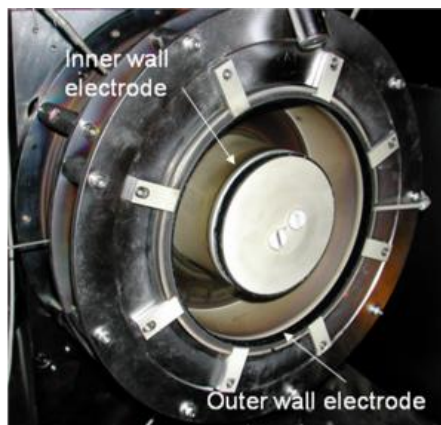


**Fig 8:** XPS spectra of smooth pre-sputtered W (dashed blue line), smooth post-sputtered W (thin black line), and W fuzz (thick red line). W fuzz has  $\text{WO}_x$  and more C and O impurities than the smooth W samples (full XPS spectra not shown).

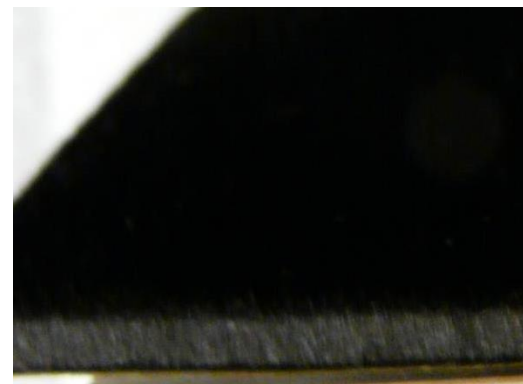
# Plasma properties can be changed by applying engineered materials to the plasma facing surface

Application of high aspect ratio carbon velvet to thruster channel walls improves considerably thruster performance by reducing the electron cross-field current and by increasing nearly twice the maximum electric field in the channel compared with the conventional BN ceramic walls.

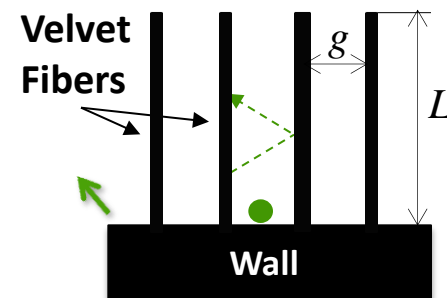
2 kW Hall thruster  
12 cm channel OD



Carbon velvet fibers:  
Diameter  $\approx 5 \mu$ ,  $L \approx 2000 \mu$ ,  $g \approx 20 \mu$



Plasma flow



Velvet suppresses SEE and reduces electron cross-field current as compared to other materials.

# Effect of anode material on the breakdown in low-pressure helium gas

To demonstrate the effect of the anode material on the breakdown in low-pressure helium gas, systematic experiments in helium were conducted using the copper cathode and a variety of materials for the anode. A wineglass discharge tube shown in the left figure was used. Results of measurements of the left sides of the Paschen curves are shown in the middle figure. The curve for graphite is substantially shifted to the right. The right figure demonstrates multi-value breakdown points for the graphite anode accessed by (1) increasing and (2) decreasing the applied voltage.

